# LUND UNIVERSITY

## Combustion Characteristics of a Swirl Dry Low Emission Burner Concept for Gas Turbine Application
### Experiments and Simulations

Kundu, Atanu

2016

[Link to publication](#)

*Total number of authors:*
1

*Creative Commons License:*
Other

# Combustion Characteristics of a Swirl Dry Low Emission Burner Concept for Gas Turbine Application

**ATANU KUNDU | FACULTY OF ENGINEERING| LUND UNIVERSITY**

# Combustion Characteristics of a Swirl Dry Low Emission Burner Concept for Gas Turbine Application

## Experiments and Simulations

Atanu Kundu

LUND
UNIVERSITY

| Organization<br>LUND UNIVERSITY | Document name<br>DOCTORAL DISSERTATION |
|---|---|
| Division of Thermal Power Engineering<br>Departmnet of Energy Science<br>PO Box 118 22100, Lund, Sweden | Date of issue<br>December 19,2016 |
| Author(s)<br>Atanu Kundu | Sponsoring organization<br>Swedish Energy Agency |

Title and subtitle

Combustion Characteristics of a Swirl Dry Low Emission Burner Concept for Gas Turbine Application: Experiments and Simulation

Abstract

In the current global energy scenario, gas turbine can provide delicate balance between the booming worlds energy requirement and a pollutant free sustainable society. Cleaner combustion of fuel (particular natural gas), efficient, reliable, low maintenance and cost effective operation of gas turbine attracted scientific community to push the limit further (high efficiency and zero emission gas turbine). Gas turbine combustion process is complex by nature as it interacts with turbulence, chemical kinetics and thermodynamics. The combined effect directly affects the component life and cost. To gain deeper understanding and develop new eco-friendly combustion technology, continuous effort has been made from last couple of decades. In the present doctoral thesis, a downscaled prototype dry low emission technology burner was extensively investigated experimentally. The thesis also aims to compare the experimental results with numerical calculations using commercial simulation tools. The main priority of the research work was to understand the flame stabilization, flame anchoring physics, the burner operational limits and emission performance. The gas turbine burner hardware was assembled with three distinct fuel and sir supply units. Along the centerline, a primary combustion zone, the RPL (Rich-Pilot-Lean) was placed. A Pilot and Main stage was placed radially outward direction from the centerline. A secondary combustion (the main flame) zone was produced downstream of the burner throat. The primary and secondary flames were stabilized by the swirling motion of the flow. Vortex breakdown and recirculation zones assisted the steady combustion process.

Several conventional measurement techniques were employed for temperature and emission (Carbon monoxide, Nitrogen oxides and unburned hydrocarbons) measurement. The experimental work in this thesis also included sophisticated optical measurement. A visually accessible liner (combustor region with diverging Quarl section) allowed optical access of the secondary flame region to analyze and record the flame characteristics. Line of sight Chemiluminescence (of hydroxyl radical), two dimensional hydroxyls radical planar laser induced fluorescence and particle image velocimetry diagnostic techniques were applied to investigate the secondary combustion (flame front and flow). All the experiments were conducted at atmospheric condition without any fuel heating. Chemical kinetic calculations were performed using CHEMKIN software for comparing the emission results. Steady and un-steady three dimensional computational fluid dynamic study was conducted using ANSYS FLUENT.

The RPL combustion produced a hot gas stream and provided radicals in to the secondary combustion zone (in the vicinity of forward recirculation zone). Initially, a dedicated experiment was conducted to explore the operability of the RPL combustor (primary zone) by varying the equivalence ratios and co-flow air properties. Results suggested that a slight rich operation could produce maximum radicals (Carbon monoxide, hydroxyls, oxygen and hydrogen radicals) without affecting nitrogen oxides emission. The main flame (secondary combustion zone) stabilization process indicated that the secondary flame was stabilized around the inner shear layer (where the incoming reactant stream and recirculated hot gas stream interacted with each other) and near the liner wall (reactant stream impinged the liner wall). The lean and rich operability limits were identified from the full burner experiments. A sharp increase of carbon monoxide concentration was noticed in the proximity of lean blowout equivalence ratio (~ 0.40). Low frequency high amplitude flame pulsation was also observed at this operating point. Flame instability and flash back tendency was observed at higher stoichiometry (~ 0.62). The Pilot and RPL stage combustion influenced the full burner flame and emission characteristics. Interaction between Pilot stages were investigated and results suggested that rich Pilot operation was helpful for stabilizing the main flame at very lean stoichiometric combustion with an emission penalty (Nitrogen oxides concentration was increased). Lean RPL operation showed emission benefits but flame instability was increased; therefore, burner operation window was compressed. Two dimensional hydroxyls radical planar laser induced fluorescence diagnostics identified the main reaction zone (captured the super-equilibrium hydroxyl concentration) and post flame region (where relaxed hydroxyl radicals were noticed in less concentration). The maximum heat release zones were identified by the Chemiluminescence imaging. An investigation of liner geometrical modification (aerodynamic variation) and its effect on flame characteristic was accomplished removing diverging Quarl geometry and replacing square liner with a circular cross section. The Quarl section demonstrated better combustion stability and wider operating window. Without Quarl, a third flame was observed from the outer recirculation zone. Outer recirculation zone flame intermittency and coupling with inner (central recirculation zone) flame structure produced high level of combustion dynamics issues. High hydrogen fuel (up to 50 % hydrogen by volume was mixed with methane) mixtures were introduced in the prototype burner. High hydrogen concentration aided a lean flame (100 K blowout benefit with 50 % hydrogen addition) operation without blowout. In addition, flow field diagnostics was carried out using two dimensional particle image velocimetry. The key flow structures (central and outer recirculation zones, shear layer, high speed swirl annular jet and vortical structures) were identified. The velocity measurement and radical concentration imaging explained the local wrinkling and dynamics of the flame structure.

A preliminary effort was demonstrated to model the full burner with numerical three dimensional calculations. Different combustion (laminar flamelet and flamelet generated manifold) and turbulence model (Reynolds-averaged Navier–Stokes, Scale adaptive simulation and large eddy simulation) were implemented in ANSYS FLUENT computation. Numerical calculation added value to the experimental results by providing a detail understanding of scalar and vector fields, especially from the locations, where optical diagnostic was not possible. The computed flame structure and flow futures were compared with the experimental results. A simplified reactor based modelling was also formulated based on computational simulation results. The aim was to investigate simulation techniques conceptually that could possibly be applied in coming studies to obtain a better numerical modeling and validation activities of turbulent gas turbine combustion design and development.

Key words: Gas Trubine Combustion, Partially Premixed flame, Flame stabilization, Swirl Flow, Emission, Experiments, Combustor, CFD, PLIF, PIV, Chemiluminescence

Classification system and/or index terms (if any)

| Supplementary bibliographical information | | Language English |
|---|---|---|
| ISSN 0282-1990 | | 978-91-7753-142-5 (print)<br>978-91-7753-143-2 (pdf) |
| Recipient's notes | Number of pages 94 | Price |
| | Security classification | |

I, the undersigned, being the copyright owner of the abstract of the above-mentioned dissertation, hereby grant to all reference sources permission to publish and disseminate the abstract of the above-mentioned dissertation.

Signature _Atanu Kr Kundu._   Date 2016-12-19

# Combustion Characteristics of a Swirl Dry Low Emission Burner Concept for Gas Turbine Application

## Experiments and Simulations

Atanu Kundu

LUND
UNIVERSITY

Cover photo by Siemens Industrial Turbomachinery AB, Sweden

(Picture of a gas turbine single can combustor)

*To almighty and my family…*

*"Everything that has a beginning has an ending.*
*Make your peace with that and all will be well."*

-Buddha

# Content

# Popular Science Description

*"I find out what the world needs. Then I go ahead and try to invent it."*

Thomas Alva Edison

As the world's, energy demand continues to grow; a thirty percent increase of global energy need is predicted for the next twenty-five years. Globally, an intense momentum on energy transition is evident from nonrenewable to renewable sources. However, at present green energy sources contributed with a minute percentage share to the global demand. Solar power contribution is less than 1 % of the electricity generation and alternative fuel/battery power technologies account for 0.1 % of the global transport system. According to the International Energy Agency (IEA), oil, coal and natural gas still account for more than 80 % of the global primary energy demand. But unfortunately, inefficient energy conversion systems (particularly from coal, which has the maximum carbon content) produces air pollution (nitrogen, carbon and sulfur oxides), climate change and global warming. It is reported that around 6.5 million premature deaths worldwide are due to the bad air quality and pollution (World Energy Outlook 2016). Recently, IEA predicted that a global shift from coal combustion to natural gas (consumption rise by 50 %) to limit the greenhouse gas emission. An efficient method to produce electricity from fuel (chemical energy) is to use the gas turbines. A gas turbine is a combustion engine that can transform natural gas or liquid fuels to mechanical energy. These combustion engines are also well known for their high reliability, low maintenance and fast startup/operational flexibility. The gas turbine is the engine at the 'heart' of the power plant that produces electric current and the combustor (where combustion process converts the chemical energy to heat) may be considered to be the 'heart' of the gas turbine. It can be assumed that the combustor pumps the heat source and boosts the fluid power for generating electricity by spinning the turbine blades. In many instances, gas turbines can be used in combination with a steam turbine to increase efficiency as a combined cycle power plant. The outstanding features (low-maintenance, high-efficiency) of gas turbine power generation has attracted global interest of natural gas-derived electricity for a sustainable society. Gas fired power generation systems are capable of reducing global greenhouse gas emissions (natural gas combustion reduces carbon dioxide emission by 50 % than coal). Economically, advanced gas turbine technology provides customers one of the lowest installed costs per kilowatt. At present, the maximum combined cycle

efficiency of a gas turbine power plant is more than 62 %. A single percent increase in gas turbine efficiency equates to millions of dollars in saving of fuel costs and tons of carbon dioxide spared from the atmosphere. For a 1 gigawatt power plant, a 1 percent enhancement in efficiency saves 17,000 metric tons of carbon dioxide emissions a year, equivalent to removing more than 3,500 vehicles from the road (US DOE report). The efficiency increment and emission reduction is challenging. A rigorous effort in engineering and technology development is essential for understanding the complex nature of these energy conversion machines. The most challenging task of all is to mix and burn the fuel efficiently, which demands a massive research and development work on combustion physics.

The combustion process is a complex phenomenon and requires understanding of underlying physics of gas turbine combustion - fluid dynamics, turbulence, chemistry, thermodynamics, aerodynamics and acoustics. Most efficient electricity generation is possible at high temperature. However, they produce higher amount of pollutant emission (nitrogen oxides) at high temperature. To reduce emission, low emission technologies are developed. The perfect fuel-air mixing and lean combustion technologies displayed high confidence on reliable, eco-friendly, efficient power generation using gas turbine. The lean combustion technology development lead to several new challenges, which includes flame stabilization, combustion pulsation/dynamics (unsteady heat release and acoustic pulsation), lean blowout and fuel flexibility problems. Apart from that, flexible generation with load variation (with distributed grid), quick startup and turndown characteristics made the new combustor development more and more challenging. Economic and environmental reasons, extended operability and fuel flexibility is important for new combustion devices. A common combustion system capable of operating with wider ranges of heavy hydrocarbons, hydrogen and inerts will have an advantage to accommodate the future fuel gas trends and provide value to gas turbine operators.

Siemen's 4th generation Dry Low Emission burner concept is developed to satisfy the gas turbine efficiency, fuel flexibility and emission compliance for a large and stable operating range. In the present work, the lab scale version of the Dry Low Emission burner was examined extensively for understanding the combustion process. Burner performance was evaluated using the prototype version, which provided insight into flame structure, anchoring and stabilization. The operational flexibility and fuel flexibility were investigated to map the emission confidence level of the burner. The optically accessible combustion chamber made possible to perform detailed experimental investigations which are difficult to perform in real engine environment. Advanced laser diagnostic techniques (Particle image velocimetry and Planar laser induced fluorescence) were employed to investigate the flow and flame. The numerical simulation work complemented the experimental results and bolstered the research and development activities of the new low emission technology burner.

# Acknowledgement

First and foremost, I would like to thank Lund University for accepting me as a PhD student. I am grateful to the Department of energy sciences and Division of Thermal Power engineering for facilitating my doctoral study and research.

I want to thank my advisor Prof. Jens Klingmann. I appreciate all his contributions of time, ideas, and guidance to make my Ph.D. experience productive and stimulating. I am also thankful for professional and personal guidance he has provided for the entire journey.

I am thankful to my co-supervisor Dr. Alessandro Schönborn for mentoring and motivating me in every moment. I would like to thank my colleagues and staff at the Department of Energy Sciences and Division of Thermal Power Engineering. A special appreciation to Prof. Magnus Genrup for his continuous support and encouragement as a friend and colleague. I am thankful to Dr. Marcus Thern, Prof. Xue-Song Bai, Prof. Öivind Andersson, Prof. Johan Revstedt and Dr. Robert-Zoltán Szász for helping me with technical and practical suggestions to encounter research problems. I am grateful to Catarina Linden, Elna Andersson, Maj-Lis Roos, Krister Olsson, Janusz Wollerstrand and Martin Carlsson for their generous help and support. I would like to express my thankfulness to Dr. Ronald Whiddon, Dr. Ivan Sigfrid, Dr. Majed Sammak, Dr. Henning Carlsson, Dr. Parisa Sayad, Dr. Ali Al Sam, Dr. Luis Teia, Pablo Garcia and Mayken Maus for their valuable inputs and help in personal and professional front.

I would like to thank all staff members at Division of Combustion physics. Particularly I want to mention my gratefulness to the person without whom the research was impossible. Thank you Mr. Rutger Lorensson ("*Du gör det omöjliga möjligt*") for fixing all the issues related to test stand and experiments. I am extremely thankful to Mr. Igor Buzuk for your great support (solving all electrical, electronics and software issues) and being a good friend. The PhD research was impossible without my laboratory partner Arman Ahamed Subash. I am grateful for his support with laser diagnostics and other numerous laboratory activities. Many thanks to Prof. Alexander Konnov, Dr. Fahed Abou Nada, Dr. Vladimir Alekseev and Dr. Elna Heimdal Nilsson for helping me with technical understanding on chemical kinetics and lasers. I express my gratitude to Dr. Per Petersson for helping me with PIV experiments. Thanks to Dr. Robert Collin and Prof. Marcus Aldén for

11

*"In the end, it's not the years in your life that count. It's the life in your years"*

Abraham Lincoln

# Abstract

In the current global energy scenario, gas turbine can provide delicate balance between the booming worlds energy requirement and a pollutant free sustainable society. Cleaner combustion of fuel (particular natural gas), efficient, reliable, low maintenance and cost effective operation of gas turbine attracted scientific community to push the limit further (high efficiency and zero emission gas turbine). Gas turbine combustion process is complex by nature as it interacts with turbulence, chemical kinetics and thermodynamics. The combined effect directly affects the component life and cost. To gain deeper understanding and develop new eco-friendly combustion technology, continuous effort has been made from last couple of decades. In the present doctoral thesis, a downscaled prototype dry low emission technology burner was extensively investigated experimentally. The thesis also aims to compare the experimental results with numerical calculations using commercial simulation tools. The main priority of the research work was to understand the flame stabilization, flame anchoring physics, the burner operational limits and emission performance. The gas turbine burner hardware was assembled with three distinct fuel and sir supply units. Along the centerline, a primary combustion zone, the RPL (Rich-Pilot-Lean) was placed. A Pilot and Main stage was placed radially outward direction from the centerline. A secondary combustion (the main flame) zone was produced downstream of the burner throat. The primary and secondary flames were stabilized by the swirling motion of the flow. Vortex breakdown and recirculation zones assisted the steady combustion process.

Several conventional measurement techniques were employed for temperature and emission (Carbon monoxide, Nitrogen oxides and unburned hydrocarbons) measurement. The experimental work in this thesis also included sophisticated optical measurement. A visually accessible liner (combustor region with diverging Quarl section) allowed optical access of the secondary flame region to analyze and record the flame characteristics. Line of sight Chemiluminescence (of hydroxyl radical), two dimensional hydroxyls radical planar laser induced fluorescence and particle image velocimetry diagnostic techniques were applied to investigate the secondary combustion (flame front and flow). All the experiments were conducted at atmospheric condition without any fuel heating. Chemical kinetic calculations were performed using CHEMKIN software for comparing the emission results.

Steady and un-steady three dimensional computational fluid dynamic studies were conducted using ANSYS FLUENT.

The RPL combustion produced a hot gas stream and provided radicals in to the secondary combustion zone (in the vicinity of forward recirculation zone). Initially, a dedicated experiment was conducted to explore the operability of the RPL combustor (primary zone) by varying the equivalence ratios and co-flow air properties. Results suggested that a slight rich operation could produce maximum radicals (Carbon monoxide, hydroxyls, oxygen and hydrogen radicals) from the RPL without affecting nitrogen oxides emission. The main flame (secondary combustion zone) stabilization process indicated that the secondary flame was stabilized around the inner shear layer (where the incoming reactant stream and recirculated hot gas stream interacted with each other) and near the liner wall (reactant stream impinged the liner wall). The lean and rich operability limits were identified from the full burner experiments. A sharp increase of carbon monoxide concentration was noticed in the proximity of lean blowout equivalence ratio (~ 0.40). Low frequency high amplitude flame pulsation was also observed at this operating point. Flame instability and flash back tendency was observed at higher stoichiometry (~ 0.62). The Pilot and RPL stage combustion influenced the full burner flame and emission characteristics. Interaction between Pilot stages were investigated and results suggested that rich Pilot operation was helpful for stabilizing the main flame at very lean stoichiometric combustion with an emission penalty (Nitrogen oxides concentration was increased). Lean RPL operation showed emission benefits but flame instability was increased; therefore, burner operation window was compressed. Two dimensional hydroxyls radical planar laser induced fluorescence diagnostics identified the main reaction zone (captured the super-equilibrium hydroxyl concentration) and post flame region (where relaxed hydroxyl radicals were noticed in less concentration). The maximum heat release zones were identified by the Chemiluminescence imaging. An investigation of combustor geometrical modification (aerodynamic variation) and its effect on flame characteristic was accomplished removing diverging Quarl geometry and replacing square liner with a circular cross section. The Quarl combustor arrangement demonstrated better combustion stability and wider operating window. Without Quarl, a third flame was observed from the outer recirculation zone. Outer recirculation zone flame intermittency and coupling with inner (central recirculation zone) flame structure produced high level of combustion dynamics issues. High hydrogen fuel (up to 50 % hydrogen by volume was mixed with methane) mixtures were introduced in the prototype burner. High hydrogen concentration aided a lean flame (100 K blowout benefit with 50 % hydrogen addition) operation without blowout. In addition, flow field diagnostics were carried out using two dimensional particle image velocimetry. The key flow structures (central and outer recirculation zones, shear layer, high speed swirl annular jet and vortical structures) were

identified. The velocity measurement and radical concentration imaging explained the local wrinkling and dynamics of the flame structure.

A preliminary effort was demonstrated to model the full burner with numerical three dimensional calculations. Different combustion (laminar flamelet and flamelet generated manifold) and turbulence model (Reynolds-averaged Navier–Stokes, Scale adaptive simulation and large eddy simulation) were implemented in ANSYS FLUENT computation. Numerical calculation added value to the experimental results by providing a detail understanding of scalar and vector fields, especially from the locations, where optical diagnostic was not possible. The computed flame structure and flow futures were compared with the experimental results. A simplified reactor based modelling was also formulated based on computational simulation results. The aim was to investigate simulation techniques conceptually that could possibly be applied in coming studies to obtain a better numerical modeling and validation activities of turbulent gas turbine combustion design and development.

# List of Publications

The thesis includes 11 research papers, which are indexed by Roman numerals. All papers are appended at the end of the thesis in chronological order.

**Paper I**

**Atanu, Kundu**, Arman Ahamed Subash, Ronald Whiddon, Robert Collin and Jens Klingmann, "Operability and performance of central (Pilot) stage of an industrial prototype burner" *ASME Power Conference 2015.*

**Paper II**

Subash, Arman Ahamed, **Atanu Kundu**, Ronald Whiddon, Robert Collin, Jens Klingmann and Marcus Aldén, "Flame Investigation of a Gas Turbine Central Pilot Body Burner at Atmospheric Pressure Conditions Using OH PLIF and High-Speed Flame Chemiluminescence Imaging" *ASME 2015 Gas Turbine India Conference. American Society of Mechanical Engineers, 2015.*

**Paper III**

**Atanu, Kundu**, Arman Ahamed Subash, Robert Collin and Jens Klingmann, "Flame Stabilization and Emission Characteristics of a Prototype Gas Turbine Burner at Atmospheric Conditions" *ASME Turbo Expo 2016: Turbomachinery Technical Conference and Exposition. American Society of Mechanical Engineers, 2016.*

**Paper IV**

**Atanu, Kundu**, Arman Ahamed Subash, Robert Collin and Jens Klingmann, "Pilot-Pilot Interaction Effects on a Prototype DLE Gas Turbine Burner Combustion" *ASME Turbo Expo 2016: Turbomachinery Technical Conference and Exposition. American Society of Mechanical Engineers, 2016.*

**Paper V**

Subash, Arman Ahamed, **Atanu Kundu**, Robert Collin, Jens Klingmann and Marcus Aldén, "Laser-Based Investigation on a Dry Low Emission Industrial Prototype Burner at Atmospheric Pressure Conditions" *ASME Turbo Expo 2016: Turbomachinery Technical Conference and Exposition. American Society of Mechanical Engineers, 2016.*

**Paper VI**

**Atanu, Kundu**, Arman Ahamed Subash, Robert Collin and Jens Klingmann, "Experimental and Numerical Investigation of a Prototype Low NOx Gas Turbine Burner" *ASME Power Conference 2016.*

**Paper VII**

**Atanu, Kundu**, Arman Ahamed Subash, Robert Collin and Jens Klingmann, " Impact of Combustion Chamber Geometry on a Partially Premixed Swirl Flame" ASME Turbo Expo 2017: *Turbomachinery Technical Conference and Exposition. American Society of Mechanical Engineers, 2017 (Submitted).*

**Paper VIII**

**Atanu, Kundu**, Arman Ahamed Subash, Robert Collin and Jens Klingmann, " Fuel Flexibility of a Multi Staged Prototype Gas Turbine Burner" *ASME Turbo Expo 2017: Turbomachinery Technical Conference and Exposition. American Society of Mechanical Engineers, 2017 (Submitted).*

**Paper IX**

Subash, Arman Ahamed, **Atanu Kundu**, Robert Collin, Jens Klingmann and Marcus Aldén, " Hydrogen Enriched Methane Flame in a Dry Low Emission Industrial Prototype Burner at Atmospheric Pressure Conditions" *ASME Turbo Expo 2017: Turbomachinery Technical Conference and Exposition. American Society of Mechanical Engineers, 2017 (Submitted).*

**Paper X**

Subash, Arman Ahamed, **Atanu Kundu**, Robert Collin, Jens Klingmann and Marcus Aldén, " Experimental Investigation of the Influence of Burner Geometry on Flame Characteristics at a Dry Low Emission Industrial Prototype Burner at Atmospheric Pressure Conditions" ASME Turbo Expo 2017: *Turbomachinery Technical Conference and Exposition. American Society of Mechanical Engineers, 2017 (Submitted).*

**Paper XI**

**Atanu, Kundu**, Arman Ahamed Subash, Robert Collin and Jens Klingmann, " Flow Field Investigation of a Dry Low Emission Swirl Burner" *manuscript ready for submission.*

# Nomenclature

| | | |
|---|---|---|
| C1 | Convective heat flux (hot side) | [W/m$^2$] |
| C2 | Convective heat flux (cold side) | [W/m$^2$] |
| D | Diameter | [m] |
| Da | Damköhler number | [-] |
| $\bar{c}$ | Mean reaction progress | [-] |
| $\overline{c'}$ | Mean reaction progress variance | [-] |
| $\bar{f}$ | Mean mixture fraction | [-] |
| $\overline{f'}$ | Mean mixture faction variance | [-] |
| $K_{1-2}$ | Conductive heat flux | [W/m$^2$] |
| Ka | Karlovitz number | [-] |
| LCV | Lower calorific value | [MJ/kg] |
| P | Pressure | [N/m$^2$] |
| R1 | Radiative heat flux (hot side) | [W/m$^2$] |
| R2 | Radiative heat flux (cold side) | [W/m$^2$] |
| Re | Reynolds number | [-] |
| $u'$ | RMS velocity | [m/s] |
| $S_L^0$ | Laminar flame speed | [m/s] |
| $S_T$ | Turbulent flame speed | [m/s] |
| SN | Swirl number | [-] |
| ST | Stokes number | [-] |
| T | Temperature | [K] |
| TKE | Turbulent kinetic energy | [m$^2$/s$^2$] |
| $Y_{fuel}$ | Fuel mas fraction | [-] |

# Abbreviations

| | |
|---|---|
| CFD | Computational fluid dynamics |
| CRN | Chemical reactor network |
| CRZ | Central recirculation zone |
| CIVB | Combustion induced vortex breakdown |
| C/S | Cross section |
| DNS | Direct numerical simulation |
| DLE | Dry low emission |
| DLN | Dry low NOx |
| EV | Environmental burner |
| ER | Equivalence Ratios |
| FGM | Flamelet generated manifold |
| FFT | Fast Fourier transform |
| HFD | High frequency dynamics |
| HRSG | Heat recovery steam generator |
| ICCD | Intensified charge-coupled device |
| IFD | Intermediate flame dynamics |
| ISL | Inner shear layer |
| LFM | Laminar flamelet model |
| LFD | Low frequency dynamics |
| LES | Large eddy simulation |
| LBO | Lean blowout |
| MFD | Medium frequency dynamics |
| MNQC | Multi nozzle quite combustor |
| Nd: YAG | Neodymium-doped yttrium aluminum garnet |
| NG | Natural gas |
| OSL | Outer shear layer |
| ORZ | Outer recirculation zone |

| | | |
|---|---|---|
| PSR | Perfectly stirred reactor | |
| PFR | Plug flow reactor | |
| PIV | Particle image velocimetry | |
| POD | Proper orthogonal decomposition | |
| PLIF | Planar laser induced fluorescence | |
| PVC | Precessing vortex core | |
| PPMVD | Parts Per Million, Volumetric Dry | |
| RQL | Rich quench lean | |
| RMS | Root mean square | |
| RPL | Rich-pilot-lean | |
| RANS | Reynolds-averaged Navier–Stokes | |
| SAS | Scale adaptive simulation | |
| SEV | Sequential environmental burner | |
| T/C | Thermocouple | |
| TIT | Turbine inlet temperature | |
| TAPS | Twin-annular pre-swirl | |
| TBC | Thermal barrier coating | |
| UHC | Unburned hydrocarbon | |
| UV | Ultraviolet | |
| ULN | Ultra low NOx | |
| URANS | Unsteady RANS | |

# Greek characters

| | | |
|---|---|---|
| $\delta_f$ | Flame thickness | [m] |
| $\delta_r$ | Inner layer thickness | [m] |
| $\tau_c$ | Chemical time scale | [s] |
| $\tau_f$ | Flow time scale | [s] |
| $\Phi_{Global}$ | Global Equivalence ratio | [-] |

| $\kappa$ | Turbulent kinetic energy | $[m^2/s^2]$ |
|---|---|---|
| $\varepsilon$ | Turbulent dissipation rate | $[m^2/s^3]$ |
| $\chi$ | Scalar dissipation rate | $[1/s]$ |

# Chemical Compounds

| $C_2^*$ | Electronically excited diatomic carbon |
|---|---|
| $CH^*$ | Electronically excited methylidyne radical |
| $CO$ | Carbon monoxide |
| $CO^*$ | Electronically excited carbon monoxide |
| $CO_2$ | Carbon dioxide |
| $CO_2^*$ | Electronically excited carbon dioxide |
| $H$ | Atomic hydrogen |
| $H_2O$ | Water |
| $N$ | Atomic nitrogen |
| $N_2$ | Nitrogen |
| $NO$ | Nitrogen monoxide |
| $NO_x$ | Nitrogen oxide |
| $N_2O$ | Nitrous oxide |
| $O$ | Atomic oxygen |
| $O_2$ | Oxygen |
| $OH$ | Hydroxide radical |
| $OH^*$ | Electronically excited hydroxide |
| $SO_x$ | Sulfur oxide |
| $TiO_2$ | Titanium dioxide |

# List of Figures

# CHAPTER 1: INTRODUCTION

## 1.1 Motivation

For a sustainable society, electricity is an indispensable parameter for social, industrial and economic growth. Modern society is extremely dependable on electricity for fulfilling industrial, residential, transportation and service related need. While the global economic rise demanded higher electricity and power generation, in developing countries around 1.2 billion people lack access to the electricity [1]. Today's energy situation and future trend shows (Figure 1.1) 80 % increase of electricity demand (in absolute terms).
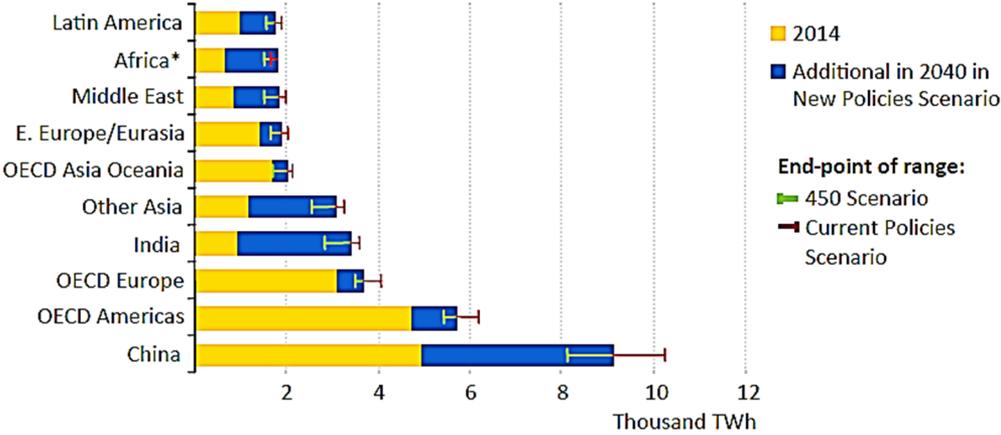


**Figure 1.1: Electricity demand by region and scenario considering different policy [1].**

The massive electricity demand and supply need deliberate balancing of policy, economical and geo-political diversity and environmental needs. According to the recent agreement in Paris [1], the "New Policies Scenario" global energy mix for the top five energy demanding regions is shown in Figure 1.2.
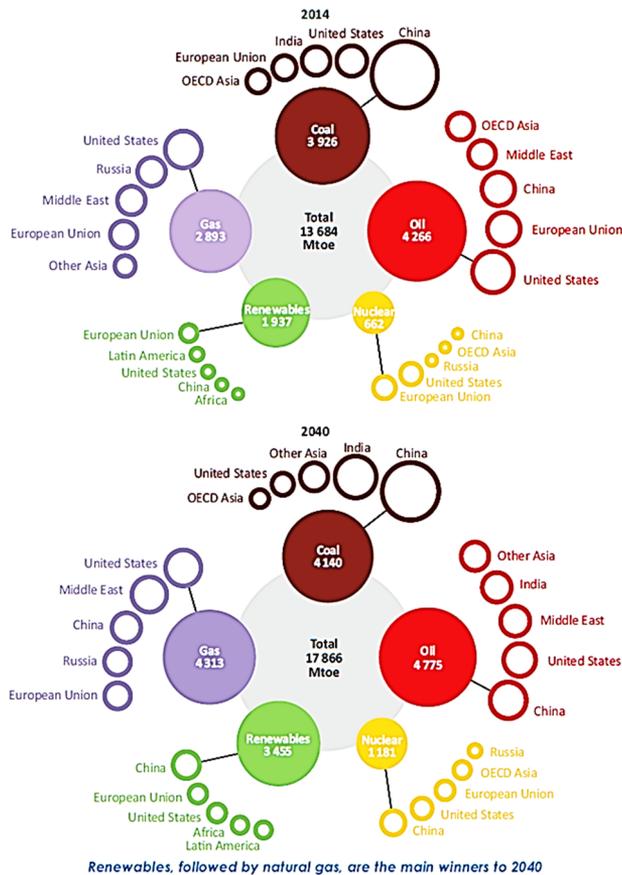
**Figure 1.2: Global energy mix, present and future scenario [1].**

The analysis clearly indicates a faster growth of renewable energy sources. However, fossil fuel contribution is significant to fulfil the massive electricity demand. As per the prediction, among the fossil fuels, natural gas consumption can be 50 % higher; whereas a reduction of coal and oil demand is predicted. Considering the world diversity and supply-demand statistics, fossil fuel contribution cannot be ignored in the near future. The most challenging task using the fossil fuel is to reduce the green house and toxic gas emission. The problem is directly related to unregulated energy production and use, poorly regulated inefficient combustion of fuel. Emission of particulate matter, $CO_2$, SOx, NOx and CO in to the atmosphere creates severe health hazards. Combustion of coal and biomass (still used for cooking in developing countries) are the main source (Figure 1.3) of air pollution (i.e. SOx, NOx and particulate matter), which leads to smog and 3.5 million premature deaths each year [1].
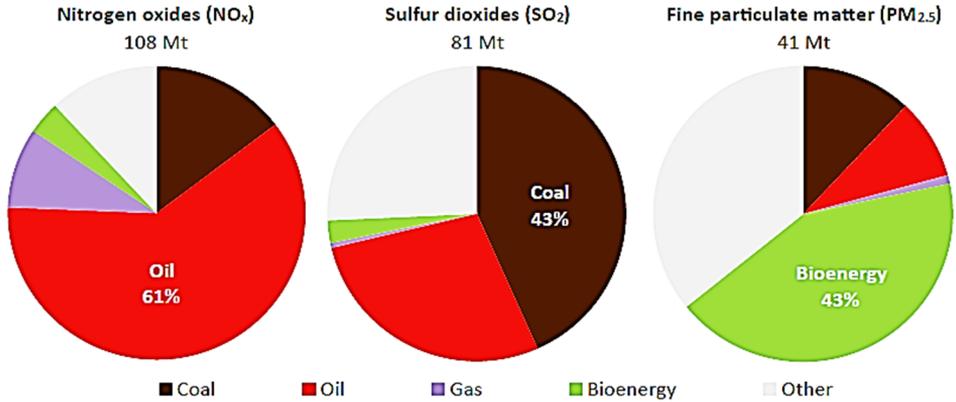
**Figure 1.3: Estimated anthropogenic emissions of the main air pollutants by source, 2015 [1].**

As a whole, at present day, meeting the global energy demand without affecting the environment (pollution reduction) is the major focus of the engineering and scientific community. Advanced technology development for clean efficient power generation and combustion system are critical for a sustainable society.

Gas turbine is one of the best available technology in the market for addressing energy demand, cost and greenhouse gas emission. The gas turbine market is not only limited to power generation. The aerospace/aviation industry, marine propulsion, defense sectors are highly dependent on gas turbines. Major gas turbine manufacturers (i.e. GE, Siemens) and government funded agencies spend billion dollars on technology development to increase gas turbine efficiency and emission reduction. Continuous research on material science, aerodynamics, heat transfer and combustion improved gas turbine simple cycle (~ 45 %) and combustion cycle (~ 62.22 %) efficiency. Historically, with the evolution of gas turbine combustor type (diffusion control to lean premixed), emission reduction technologies (water and steam injection) are also evolved. New emission reduction technologies (EV, SEV, ULN, DLN and DLE) are capable of reducing the NOx emission level below 9 ppm.at higher turbine inlet temperature [2, 3]. In the last decades, laboratory scale combustor research (experimental and numerical) supported new technology development with fundamental studies, complex diagnostics, modelling and high fidelity numerical simulations. Detailed experiments with unique visualization capability of lab scale combustion chamber enhanced the understanding of combustion process, its stabilization and static and dynamical properties with high degree of confidence [4, 5]. Advanced laser diagnostic techniques are applied for exploring internal flame structure, reaction zones and the complex flow-flame interactions [6-9]. Simultaneously, combustion, turbulence and numerical model development provided extra thrust in gas turbine (combustion and flame) research

(DNS and LES) [10-13]. Laboratory testing and product development capabilities are extended significantly using the simulation and high performance computing. New concept development (power generation and propulsion sector) for burner/nozzle development (i.e. flame sheet combustor , late staging concept, lean premixed TAPS and RQL) enhanced the gas turbine operational capability and fuel flexibility without compromising on emission [14-16]. Several parameters are associated with a new burner development need to be concerned about. The flame stabilization is a challenging process for a fuel flexible operation (LCV and high hydrogen content fuels) [17]. The combustion process inside gas turbine is highly sensitive to the geometry. The slight modification of geometry can alter the burner aerodynamics and mixing profile, which inherently affects the burner emission performance and operability. A strong interaction between flame, flow-field and instability is observed from experiments [18, 19]. The lower flame temperature combustion is generally susceptible to the instabilities (LBO and combustion dynamics). All these factors (extremely complicated and interlinked) are critical for designing a new combustion system. Considering the non-accessibility (optical visibility and laser diagnostics) and complexity (high pressure and load) of the real gas turbine engine running in the field, laboratory scale experiments provided a great deal of information (flame and flow) using model or prototype combustor. The experimental/simulation results can be applied directly or indirectly (used as model development and CFD validation) for new combustion technology development.

In this thesis, experimental and numerical investigations conducted on a laboratory scale prototype 4th generation DLE burner (designed and developed by Siemens Industrial Turbomachinery AB, Sweden) are described. The new burner concept is based on aerodynamic flame stabilization with the help of swirl flow and vortex breakdown. A swirl burner design can produce excellent fuel-air mixing in a short residence time. A shorter flame shape and flame stability could be improved utilizing the aerodynamic flow structure [20]. The flame macro structure provides the detail information of flame anchoring, its length and heat release region. Thermal heat load on the combustor wall, cooling flow and local flame quenching are directly affected by the flame stabilization. The flame anchoring and stabilization process were experimentally investigated using different optical diagnostic techniques (diverging Quarl and liner was optically accessible). It is a known fact that Pilot flames are essential for better flame stability at part load and lean operation [21]. Investigation of fuel partitioning through Pilot and RPL showed direct relationship between emission and Pilot flame combustion. The Variation of operating condition and burner staging effect (Pilot and RPL) investigations were extremely important to define the operational stability of the burner in the lean and rich operating regime. Apart from that, the burner staging concept is important for multiple fuel (Wobbe Index variation) handing capability without shifting the flame stabilization/heat release location. The local equivalence ratio modification, flow

and flame interaction can trigger combustion pulsation problem. This could damage the burner hardware and initiate an unwanted trip of the gas turbine. Aerodynamic stability and fuel flexibility tests showed the burner operational robustness. Numerical analysis (chemical kinetic calculation and CFD modelling) was very important in order to obtain a better understanding of gas turbine combustion.

## 1.2 Thesis Objective

The primary objective of this thesis was understanding the DLE burner concept in detail using experimental and numerical tools. The macro structure of the flame (stabilization, anchoring, shape and length) required to be explored using optical diagnostic tools. Flow field investigations were aimed at shedding light on the highly swirled turbulent combustion flow field. Burner stable operability window (lean blow out and flashback) and emission characteristic mapping were required to be identified using different fuels and combustor geometries. Based on experimental and conceptual computational study, model validation was to be conducted by comparing OH-PLIF, emission and PIV results.

## 1.3 Methodologies

An atmospheric experimental setup was built at Division of Combustion Physics laboratory of Lund University. The first test was designed to explore only the RPL (central stage of the burner, acted as a small Pilot) combustion section. In this experiment, Pilot fuel and Main stage (fuel and air supply) hardware was eliminated. Thereafter, for all the experiments same experimental setup (with full burner) was utilized. The following measurements were conducted with collaboration of Division of Combustion Physics, Lund University.

- Temperature was monitored from the RPL outer wall and combustor exit using B, N and K Type T/C's. Additional T/C's were placed for monitoring air preheat, reactant temperature at burner throat location, liner head end and exhaust gas temperature.

- Emission measurement was performed from the liner exit using a water cooled multi holed probe. Primarily, NOx, CO and UHC concentrations were tracked.

- High speed (up to 4700 Hz) and low speed (10 Hz) OH Chemiluminescence imaging for identifying the maximum heat release region.

- The flame front (including post flame zone) location was visualized by the OH-PLIF system (10 Hz).

- Flow field measurement using a 4 Hz 2D PIV system.

- Liner cross section was varied from square C/S to circular C/S. The diverging Quarl geometrical section was eliminated (defined as Dump combustor) and compare with Quarl case (the Baseline).

- Methane (99.5 % pure) was used as fuel for baseline condition. In the later stage up to 50 % Hydrogen (by volume) was blended with methane gas. The natural gas supplied to the laboratory (Lund City NG grid) was also used for testing.

Apart from that numerical simulations were performed.

3D CFD simulation of the full burner (360 degree) was conducted using 14 million (RANS and SAS) and 22 million (LES) polyhedral cells. The mesh included the fuel and air supply holes, swirl vanes and cooling slots. A mesh sensitivity study was conducted for the baseline case.

Simplified chemical reactor network (CRN) model was constructed using the CFD calculated flow split information, PSR and PFR. One dimensional heat loss calculation (conduction, convection and radiation) was incorporated with the CRN model to predict correct emission (CO and NOx).

## 1.4 Limitations

The research work included in this thesis suffers from following drawbacks

- No high pressure experiment was conducted.

- The primary flame (RPL) was not visually accessible.

- Simultaneous flame and flow diagnostic was not performed.

- No dynamic pressure measurement was possible to capture instabilities.

Detailed CFD calculation using different combustion, NOx and turbulence model was not performed. Model validation and optimization require further investigation in future.

# 1.5 Thesis Outline

This doctoral thesis is comprised with six chapters followed by six published, four submitted and one ready to submit research papers.

**Chapter 1**

Thesis introduction with background information for the research work. Research approach and limitations are also included.

**Chapter 2**

The fundamentals of gas turbine combustion system. Advanced combustion system design requirement and challenges are described briefly. This chapter also includes the fundamental aspects of turbulent gas turbine combustion.

**Chapter 3**

The industrial burner component and flow path is described here. The atmospheric test facility and instrumentation diagram are presented.

**Chapter 4**

Optical and laser diagnostic techniques are introduced in this chapter. Basic principle of Chemiluminescence, OH-PLIF and PIV diagnostic techniques are described briefly. This chapter also describe the CFD simulation methods and models applied in the thesis. Theoretical background of CRN modelling with PSR and PFR is discussed. One dimensional heat loss calculation method is described.

**Chapter 5**

Key results from experiment and simulation are highlighted. Summary of the research publication is attached here.

**Chapter 6**

Main conclusions of the research work are presented with future scope.

# CHAPTER 2: GAS TURBINE COMBUSTION SYSTEM

## 2.1 Gas Turbine Power Generation

The power generation sector uses gas turbine as a main technology for converting fossil fuel energy (chemical) to electricity. The combination of gas turbine with steam and HRSG called as combined cycle power plant showed high efficiency and reliability. The clean conversion process of chemical energy in to electricity in gas turbine gradually replacing coal and oil fired gas units globally. A combined cycle power plant layout is depicted in Figure 2.1. The gas turbine drives a generator and the remaining thermal energy is extracted from the exhaust gas in HRSG. The HRSG is a boiler where water is converted to steam, which drives the steam turbine to produce more electricity (same coupled generator for gas and steam turbine).



**Figure 2.1: Combined cycle power plant.**

1) Gas Turbine 2) Generator 3) Steam Turbine and 4) Heat Recovery Steam Generator (Source: GE Power).

The operating principle of gas turbine can be understood from Figure 2.2. A thermodynamics cycle (named Brayton cycle) represent the gas turbine operation. The cycle comprises of four processes, as shown in Figure 2.2. From P-V and T-S diagram represent the thermodynamic property change of the working fluid. The ambient air is compressed isentropically (in ideal case) in the compressor section, therefore pressure and temperature of the air is increased (state 1 to state 2). In the next stage inside combustor, heat can be added at constant pressure (owing to fuel-air combustion, from state 2 to state 3). The high temperature gas is expanded isentropically in the turbine section (conversion of chemical energy to mechanical, from state 3 to state 4). For a closed gas turbine cycle, the exhaust gas can be cooled (constant pressure heat loss) and recirculated (state 4 to state 1) [22]. It can be noted that the cycle cannot be operated without addition of heat, which makes the combustion chamber so important.
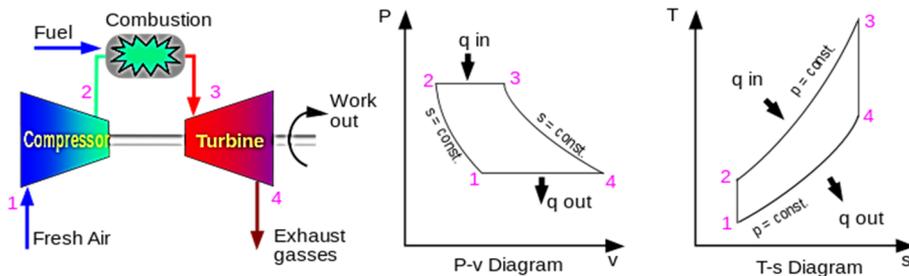


**Figure 2.2: Gas turbine cycle and components[23].**

Pressure (P) - volume (v) diagram and temperature(T) - entropy (s) digram for Brayton cycle. 'q' represents the heat addition and subtraction.

Before moving further, it is very important to understand the performance of a gas turbine cycle. Fundamentally pressure ratio and combustor outlet temperature (TIT or firing temperature) defines the gas turbine performance envelop. Figure 2.3 explains the simple cycle and combined cycle efficiency in terms of power output, efficiency and Firing temperature (combustion product gas temperature after first stage nozzle). The figure explains that a simple cycle gas turbine efficiency could be increased with the increase of pressure ratio (keeping same firing temperature). Whereas, in a combined cycle operation pressure ratio shows less pronounced effect. On the other hand, increasing the firing temperature (at same pressure ratio) increases the power output. But the extra cooling requirement shows a reduction of efficiency. In simple cycle arrangement, higher power output can be achieved with high efficiency if both firing temperature and pressure ratios are increased simultaneously. Interestingly, the combined cycle efficiency could be increased with firing temperature. It can be seen that optimum performance parameters are different for each (simple or combined) cycle.
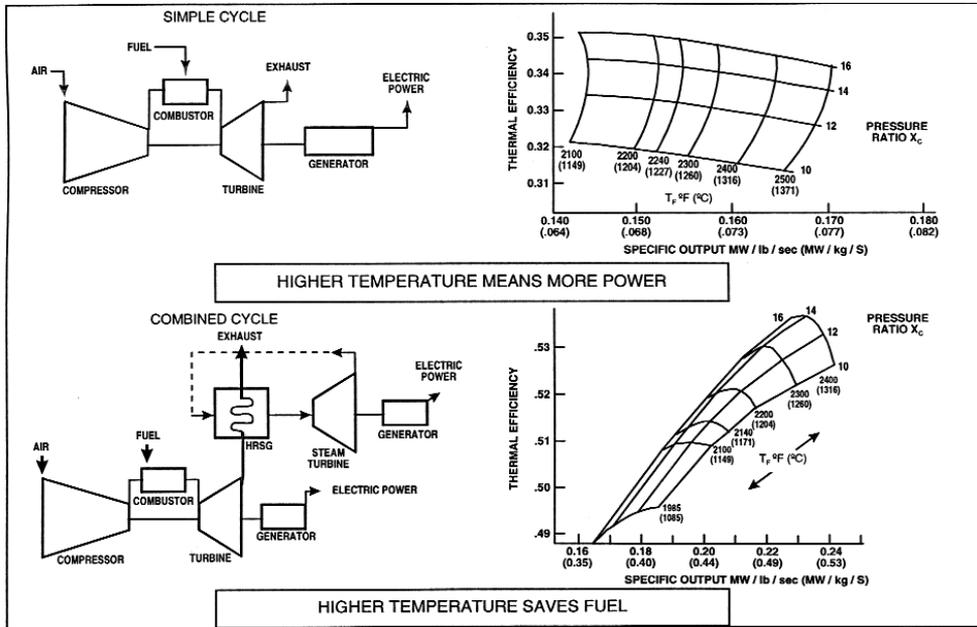
**Figure 2.3: Simple cycle and combined cycle efficiency [24].**

## 2.2 Combustor Design Challenges

As discussed in the previous section, combustion chamber is an essential, perhaps the most important component of the gas turbine operation. The combustion system design includes design of fuel-air mixing device, stable burning, required dilution and cooling to match the exit profile. A gas turbine combustion system consists of two main hardware components. The burner or fuel nozzle section (single or multiple) and the combustor (liner and transition section). The cross section of Siemens ULN combustion system is shown in Figure2.4. The fuel-air mixing process is done by the burner or nozzles. To extend the burner operability and fuel flexibility multiple nozzles are used. The fuel air mixture is burned inside the combustor. The stable flame is located inside the cylindrical liner section. Later the high temperature gas stream is directed to the turbine section using a transition stage. The main design features of a nozzle/burner system are [25]

- Safe and reliable operation for entire load range by avoiding unsteady phenomena (combustion dynamics, lean blowout, auto ignition, flashback and flame holding).

35

- Highest combustion efficiency and complete combustion (mix the fuel and air for lean premixed system using various mixing techniques i.e. multi holes and swirl device).
- Low emission (lean flame produce lower flame temperature and NOx).
- Fuel flexibility (stable flame anchoring for different fuel application and load range).
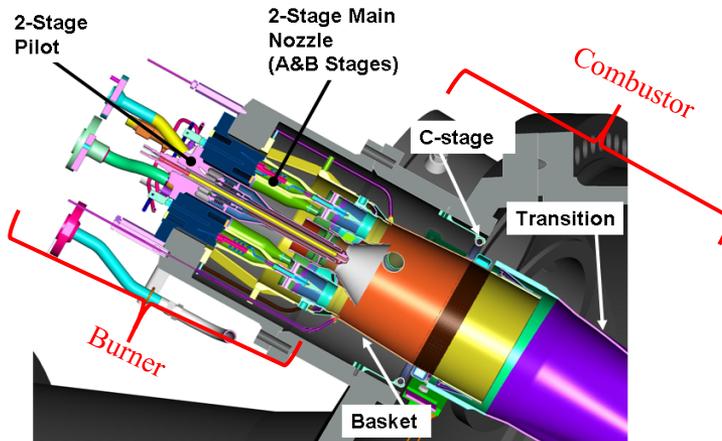


**Figure 2.4: Major components of a ULN combustion system [26].**

The combustor section provides the geometrical boundary of the flame zone to direct the heat energy towards the turbine section. The combustor section design requirements also need to be fulfilled. They are

- Compact space and optimum length to minimize CO and NOx emission.
- Aerodynamic design for less cooling flow requirement while maintaining target firing temperature.
- Minimum pressure drop across the combustor.
- Uniform thermal loading on the liner wall.
- Acceptable profile and pattern factor at the combustor outlet.
- Stable combustion and high mechanical integrity.

In the present thesis most concentration was given to the burner/nozzle section. The following parameters were targeted to analyze by experiments and simulations.

- Flame stabilization.
- Burner operability and load variation.
- Emission performance calculation.
- Burner fuel flexibility.
- Liner geometrical (aerodynamic) design modification.

## 2.3 The Flame

There are three types of flame is possible in an industrial gas turbine combustion system. Diffusion (non-premixed), premixed and partially premixed. Nowadays, the usage of diffusion type of combustors is limited as it produces high flame temperature and NOx (but can show high flame stability). The emission level could be controlled by injecting water and steam near the flame zone. The diffusion flames are used as Pilot to control the flame stability at lean operating conditions (GE MNQC for hydrogen flames [17]). In military aircraft engine and in afterburner diffusion type of flame can be used for high power requirement.

In recent days, maximum gas turbine combustion runs in premixed or partially premixed mode. These type of flames can produce less emission (higher fuel-air mixing produces low NOx [27]) and provide best combustion efficiency. The premixed flame characteristics can be understood from Figure 2.5.
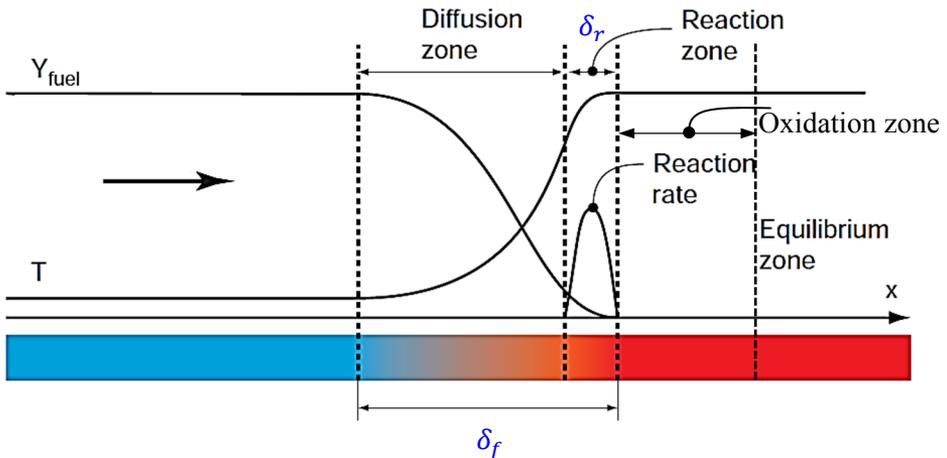


**Figure 2.5: A stationary steady laminar premixed flame [28].**

The fundamental physics of laminar premixed flame is well described in [29, 30]. In this simplified model, fuel and oxidizer is perfectly mixed prior to the combustion process. The one dimensional flame is represented by Figure 2.5. The fuel mass ($Y_{fuel}$) fraction and reactant mixture temperature (T) is constant at far upstream of the flame. The flame region is divided in four zones: the preheat or diffusion zone, the reaction zone (flame inner layer), oxidation zone and equilibrium zone. Continuous heat and radical diffusion is expected in the preheat region. The main heat release occurs in the reaction zone. The inner layer flame structure is thin ($\delta_r$) compared to the total flame thickness ($\delta_f$). For most premixed flame, the ratio of total flame thickness and inner layer thickness is around 10 [31]. In the equilibrium

region, it can be assumed that all chemical species have reached an equilibrium condition.


## 2.4 Flame-Turbulence Interaction

The laminar premixed flame structure (discussed in previous section) is highly influenced by the turbulent flow (the unburnt fuel-air mixture stream). The laminar flame front can be wrinkled or distorted by the turbulent eddies. The effect of turbulence-flame interaction is defined by laminar flame speed ($S_L^0$), laminar flame thickness ($\delta_f$) are compared with integral length scale of turbulence ($l_t$) and RMS velocity ($u'$), which represent the turbulent kinetic energy. This is called the regime diagram or Borghi diagram [30, 31]. The regime diagram based on [30] is shown in Figure 2.6.
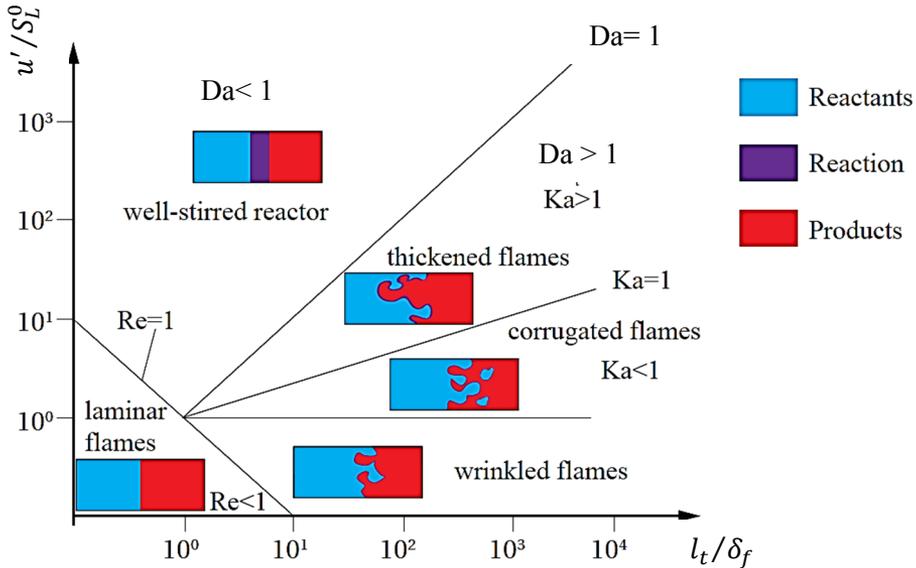


Figure 2.6: Classical premixed turbulent combustion regime diagram [32].

The Damköhler number (Da) is defined by the ratio between integral time scale, $\tau_t$ (largest eddy) to the chemical time scale, $\tau_c$ as [31]

$$\text{Da} = \frac{\tau_t}{\tau_c} = \frac{l_t/u'}{\delta_f/S_L^0} = \left(\frac{l_t}{\delta_f}\right)\Big/\left(\frac{u'}{S_L^0}\right)$$

The Karlovitz number (Ka) relates the smallest eddy (Kolmogorov) time scale ($\tau_k$) and chemical time scale as [31]

$$\text{Ka} = \frac{\tau_c}{\tau_k} = \left(\frac{l_t}{\delta_f}\right)^{-1/2}\left(\frac{u'}{S_L^0}\right)^{3/2}$$

Turbulence Reynolds number (Re) is also defined based on length scale as [31]

$$\text{Re} = \left(\frac{l_t}{\delta_f}\right)\left(\frac{u'}{S_L^0}\right)$$

The relation between Re, Ka and Da is given by

$$\text{Re} = (\text{Da})^2(\text{Ka})^2$$

According to Figure 2.6 and Da number formulation, when Da >> 1, chemical time scale is small compared to the flow time scale. In this regime, the inner structure of flame remains laminar but can be wrinkled by the turbulent motion. This regime is defined as laminar flamelet regime. The flame is thinner than the turbulent scales. When the turbulent fluctuation is larger than the flame speed, the turbulent motion can wrinkle the flame front and can produce pockets of fresh and burnt gas. This regime is defined as corrugated flamelet regime. In the thickened flame regime, turbulent scales are small and can enter the flame front. In this situation Kolmogorov scales are smaller than flame thickness, hence the flame is altered by the turbulence. Finally, when Da << 1, turbulent mixing is fast compared to chemical time scale and the regimes tends towards the well stirred reactor (PSR).

In the flamelet regime turbulent motion modifies the laminar flame speed by wrinkling the flame front [31]. The relationship between laminar and turbulent flame ($S_T$) speed is

$$\frac{S_T}{S_L^0} \approx 1 + \frac{u'}{S_L^0}$$

The turbulent flame speed can be increased by large velocity fluctuations. In real gas turbine engines and in the experiments presented in this thesis, the flow field is highly turbulent. The local flame structure is altered by turbulent eddies. The flamelet concept assumption was made while performing the numerical simulations.

# 2.5 Swirl Flame Stabilization

The flame anchoring in desired location (combustor) is essential for a gas turbine combustion system. Any deviation of flame stabilization can enormously affect the combustor life (high thermal stress) and develop dynamics issues (also affects the emission). The incoming reactant flow velocity from the burner/nozzle is generally high. To sustain the combustion process, aerodynamic blockage could be produced for facilitating the flame in the anchoring point. This process increases the reacting time and un-interrupted combustion can occur. Different types of flame stabilization

(rim stabilization, pilot flame stabilization, dump geometry stabilization, bluff body and swirl stabilization) process could be found based on variety of applications [31]. For lean premixed flame, swirl stabilization is widely accepted flame stabilization mechanism [5, 33-35]. The properties of swirling flow are

- Swirling flow generates a natural radial pressure gradient caused by axial decay of tangential velocity.

- This causes a negative axial pressure gradient in the vicinity of the central axis, which in turn induces recirculation flow and the formation of a CRZ.

- The central vortex core can become unstable, giving rise to the oscillation phenomena of the CRZ referred as PVC [36].

- The formation of the CRZ is thus dependent on the decay of swirl velocity as swirling flow expands in radial direction.

When the swirl intensity is high, Swirl number (SN) is larger than 0.5, a vortex breakdown phenomenon can occur (in Figure 2.7). The picture explains the motion and topologies of the PVC. The tangential velocity component aligns the vortex with the central axis of the combustion chamber. The vortex breakdown can be observed from the stagnation point (S) generating a spiral motion. The CRZ is located inside the spiral helical structures [37]. The entire structure rotates around the axis of the combustion chamber with PVC frequency. At the same time, a negative axial velocity can be observed from the recirculation region (low speed zone), which is used to stabilize the flame. This process is explained in detail in [38].
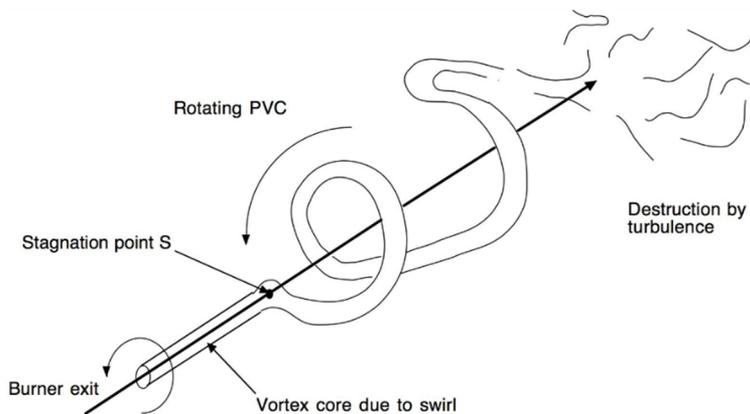


**Figure 2.7: Precessing vortex core topologies inside a combustor [31].**

# 2.6 Combustor Operability Issues

The lean premixed gas turbine combustion system operation method is bounded by (1) lower NOx emission (2) sufficient residence time for CO oxidation (3) stability at part load operation and (4) acceptable combustion dynamics. Several transient phenomena (i.e. flashback) can damage the combustion system hardware and trip the gas turbine (flame blowout).

Flashback happens when the flame propagates upstream direction of a premixed flame into a region not designed for the flame to exist. Several mechanisms can drive the flashback mechanism such as 1) flame propagation in the high-velocity core flow defined as CIVB type flashback [39] 2) flashback induced by combustion instabilities and 3) flashback in the boundary layer [28]. These mechanisms are strong function of fuel composition, operating conditions, and fluid dynamics. The detailed mechanism can be found in [40, 41]. When instantaneous axial flow velocity drops below the turbulent flame speed, combustion instability-induced flashback (high amplitude flame osculation) can be observed. The transient flame propagation inside the burner premixing section (mixing tube and swirl vane section) is detrimental and can cause total damage of the combustion system. Generally, from a combustor designer's point of view, a high axial velocity in the premixing section is desirable for pushing out the upstream propagated flame.
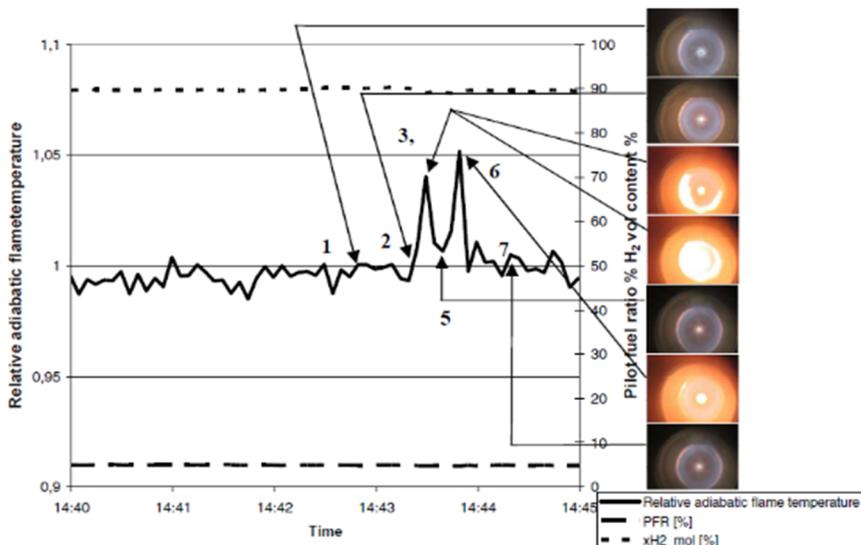


**Figure 2.8: Flashback induced combustion instability [42].**

Flameholding occurs when, the system fails to clear the flame out from the premixing section. This is a highly undesirable condition for gas turbine combustion and required measure to be considered in design phase (setting design margin to avoid Flameholding and flame flashback). Turbulent flame speed can be increased when higher amount of fuel is supplied to the combustion system. The rich stoichiometry flame and hydrogen blended (due to high diffusion properties and higher flame speed) flames are more prone to flashback instabilities. Figure 2.8 shows the flashback event recorded in an atmospheric test using SGT-750 burner (4th Generation DLE) at higher flame temperature.

Lean blowout flame instability is related to the local quenching of the flame in the highly turbulent regions, which can result in the release of partially oxidized fuel i.e. unburned hydrocarbons (UHC) and CO. The excess amount of air and high strain (produced by swirl flow) initiate the instability process. According to the literature, the LBO event is related to PVC oscillation frequency and shear layer flame de-stabilization process (due to high strain) [43]. Generally, the LBO instability shows low frequency pulsation but can have high amplitude.

These instability issues can be identified by accumulating dynamic pressure oscillation from the combustor. Three main ranges of frequencies are observed from different industrial heavy duty gas turbines. Figure 2.9 shows different bands of frequencies related to combustor.
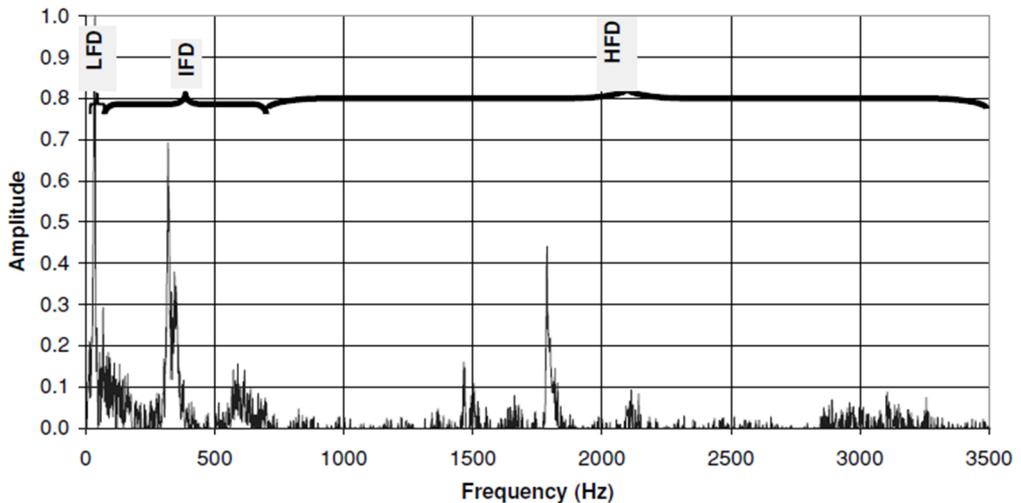


Figure 2.9: Dynamic pressure response of a single burner experiment at high pressure [44].

The low frequency dynamics (LFD), sometime defined as rumble can be found between 10-50 Hz. These type of oscillations are referred to as "cold tones," since their amplitude can be increased as the flame temperature decreases (mainly observed at very lean conditions near blowout). Intermediate or Mid frequency dynamics (IFD/MFD) can be observed between 100 - 250 Hz. They are defined as "hot tones" because their amplitude often increases with flame temperature and engine power output (this can be influenced and triggered by flame flashback). The third high frequency dynamics (HFD or screech) is occasionally observed in industrial gas turbines (beyond 1000 Hz). This type of instability is destructive (when it is with hardware resonance) and can damage engine hardware within very short time [44].

## 2.7 Fuel Flexibility

Based on fuel availability and global demand of low emission power generation, clean alternative fuel application in gas turbine is increasing day by day. Based on geographical location, fuel composition, quality and availability shows high degree of spread. Figure 2.10 shows the variety of fuels can be burnt in a gas turbine combustion system.



DO #2
Biodiesel
Condensate
Naphtha
Alcohol
Kerosene
DME
ASL
AXL
Light Crude Oil
Medium Crude Oil
Heavy Crude Oil
HFO

NG
LNG
LPG
Lean Methane
Hydrogen Blends
High Hydrogen
Ethanol
Syngas
Steel Mill Gases
Sour Gas
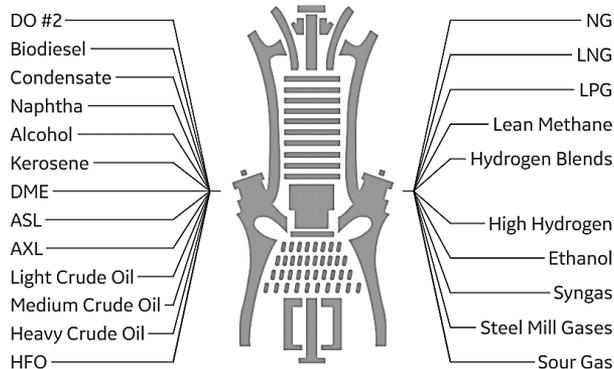
**Figure 2.10: gas turbine fuel flexibility [45].**

The combustion system primarily faces following challenges with fuel variation [17]

- Natural gas (most common fuel) optimized combustors need to be adapted to these fuels.

- Variations in the fuel composition could have operability issues [46].

The flame stability, emission can be affected by the fuel composition change. The flame instabilities might arise with fuel change (high hydrogen fuel is prone to flashback). The influence of fuel composition on flame is described in Figure 2.11.
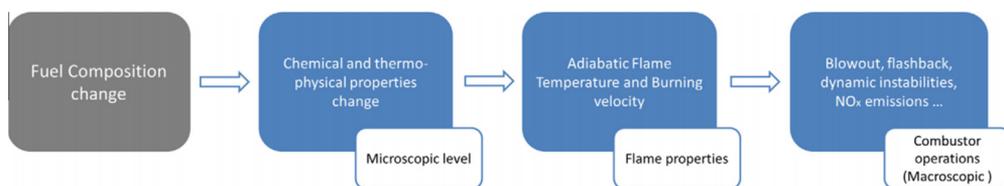


**Figure 2.11: Effect of fuel composition on flame operability [17].**

# 2.8 Gas Turbine Pollutant Emission

The combustion process involves chemical transformation of fuel hydrocarbons with the presence of atmospheric oxygen. The chemical composition of fuel molecule determines the type of oxides can be formed from the gas turbine combustion system. The pollutants are bad for the environment as well as for human health. The Figure 2.12 enlisted the pollutants can be found from gas turbine exhaust.

| Major Species | Typical Concentration (% Volume) | Source |
|---|---|---|
| Nitrogen ($N_2$) | 66 - 72 | Inlet Air |
| Oxygen ($O_2$) | 12 - 18 | Inlet Air |
| Carbon Dioxide ($CO_2$) | 1 - 5 | Oxidation of Fuel Carbon |
| Water Vapor ($H_2O$) | 1 - 5 | Oxidation of Fuel Hydrogen |
| **Minor Species Pollutants** | **Typical Concentration (PPMV)** | **Source** |
| Nitric Oxide (NO) | 20 - 220 | Oxidation of Atmosphere Nitrogen |
| Nitrogen Dioxide ($NO_2$) | 2 - 20 | Oxidation of Fuel-Bound Organic Nitrogen |
| Carbon Monoxide (CO) | 5 - 330 | Incomplete Oxidation of Fuel Carbon |
| Sulfur Dioxide ($SO_2$) | Trace - 100 | Oxidation of Fuel-Bound Organic Sulfur |
| Sulfur Trioxide ($SO_3$) | Trace - 4 | Oxidation of Fuel-Bound Organic Sulfur |
| Unburned Hydrocarbons (UHC) | 5 - 300 | Incomplete Oxidation of Fuel or Intermediates |
| Particulate Matter Smoke | Trace - 25 | Inlet Ingestion, Fuel Ash, Hot-Gas-Path |
| | | Attrition, Incomplete Oxidation of Fuel or Intermediates |

**Figure 2.12: Gas turbine exhaust emission from conventional fuel combustion [47].**

## 2.8.1 NOx Emission

The NOx is mainly formed from the combustion air (79 % nitrogen and 21 % oxygen in air by volume) at high flame temperature. The NOx formation can be

- increased rapidly with flame temperature (higher firing or TIT).
- increased with higher compressor outlet air temperature.
- increased with the square root of the combustor inlet pressure.
- increased with combustor residence time (long combustor more NOx).
- decreased with steam and water injection, heat loss effect (local quenching of flame reduce flame temperature).
- decreased with higher degree of fuel-air mixing.
- decreased with combustion staging and premixed piloting.
- decreased by reducing local oxygen concentration for NOx formation (EGR).

There are four primary chemical pathways for NOx formation.

- Thermal NOx
- Prompt NOx
- $N_2O$ route
- NNH path

The contribution of different pathways in combustion can be visualized from Figure 2.13.
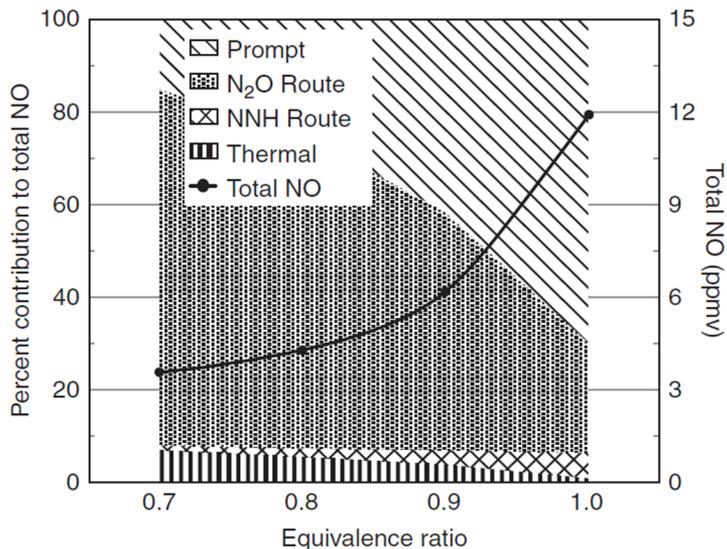


**Figure 2.13: NOx contribution from different pathways as a function of equivalence ratios for Ethane flame at 6 atm pressure [48].**

## 2.8.2 CO Emission

Formation of CO is associated with partial oxidation of fuel molecules. This can be high during gas turbine ramping, part load operation, start-up and during flame instability. The CO concentration can be higher when a gas turbine is operated near the lean blowout limit. At higher flame temperature, dissociation of $CO_2$ to CO is increased towards equilibrium, which lead to an increase of CO emission. Figure 2.14 illustrates CO emission from GE 7EA heavy duty gas turbine.
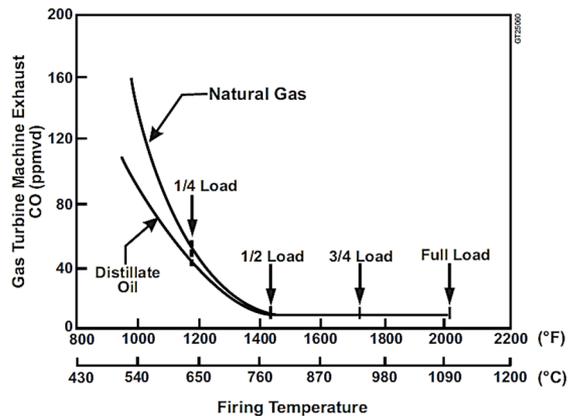


Figure 2.14: CO emission from 7EA gas turbine [47].

The reduction of gas turbine emission is mainly dependent on better combustion system design and cleaner fuel [47]. Figure 2.15 shows the different techniques for controlling gas turbine emission. Post combustion capture can decrease the emission level with an extra installation cost.

| | |
|---|---|
| $NO_x$ | Lean Head End Liner<br>Water or Steam Injection<br>Dry Low $NO_x$ |
| CO | Combustor Design<br>Catalytic Reduction |
| UHC & VOC | Combustor Design |
| $SO_x$ | Control Sulfur in Fuel |
| Particulates & PM-10 | Fuel Composition |
| Smoke Reduction | Combustor Design<br>- Fuel Composition<br>- Air Atomization |
| Particulate Reduction | Fuel Composition<br>- Sulfur<br>- Ash |

Figure 2.15: Gas turbine emission control strategy [47].

46

# CHAPTER 3: EXPERIMENTAL TEST RIG

## 3.1 SGT-750 Industrial Gas Turbine and Combustor

The new Siemens gas turbine derivative (SGT-750) is a twin-shaft machine with high performance and minimum downtime. It can be operated in simple cycle, combined cycle and cogeneration mode [49]. This type of gas turbine engines is designed and developed for distributed power generation, industrial companies (need for an independent power source) and oil & gas sector.
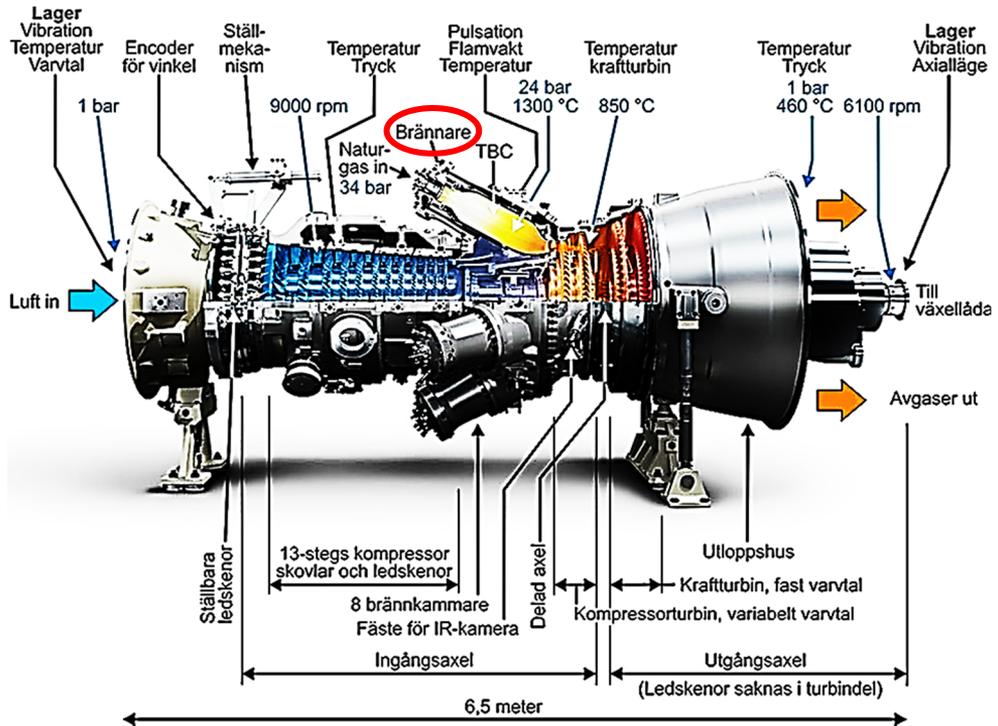


**Figure 3.1: Various Components of Siemens SGT-750 Industrial gas Turbine [50].**

This machine is equipped with the latest 4th generation DLE combustion system with less than 15 ppmvd NOx emission performance capability [51]. The gas turbine contains 13 staged axial compressor section, combustor and two air cooled turbine stages (Figure 3.1). The high pressure and temperature air stream from compressor exit takes an 180° turn and flow through the annulus section between the combustor outer casing and the liner. The SGT-750 comprises a total of 8 can combustors. A TBC coating is applied on the liner inner surface to avoid hardware overheating and damage. In the top most (left side) location of the can combustor, the DLE burner (encircled by red line in Figure 3.1) is attached for mixing the compressed air with fuel using swirl vanes.

The can combustor and burner picture is enlarged and shown in Figure 3.2 (4th generation DLE Generation 1). The combustor liner helps to complete the combustion process and guides the hot combustion product to the turbine section through a T-duct (transition) section. The DLE system is incorporated with four stages (Main 1, Main 2, Pilot and RPL). Along the burner centerline, the RPL burner is positioned at the core of the burner. The main function of this stage is to produce a hot gas stream with high concentration of radicals (OH, O, H and CO) while operating in rich condition [52]. The pilot burner is constructed around the RPL combustor. Two Main stages (M1 and M2) are located around the Pilot stage and fuel was delivered separately in to these stages using dedicated fuel manifolds [42].



*RPL = Rich-Pilot-Lean
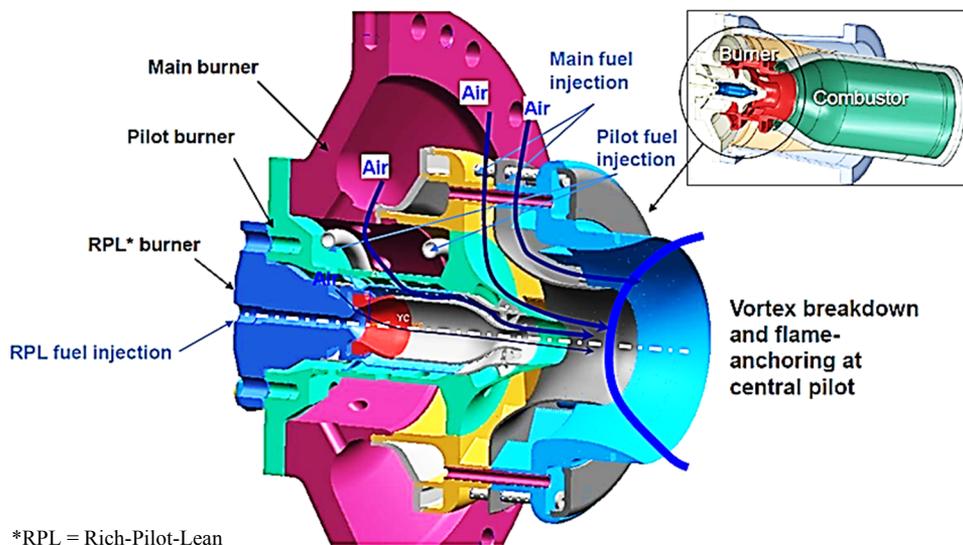
pFigure 3.2: Combustor and DLE Burner (Generation 1) for SGT-750 engine [53].

# 3.2 Downscaled Prototype Burner

The engine burner (single can) was scaled down with power for a suitable laboratory environment operation. The outermost stage "Main 1" was removed from the downscaled version. In the new test burner (generation 2) hardware, a few modifications were associated with compared to its predecessor prototype version (generation 1). The major modification was

- Fuel injection position was moved for the Pilot stage. In the new geometry, the hollow axial swirl vanes (assembled with fuel supply holes) are responsible for fuel injection (indicated as location 'A' in Figure 3.3).

- Downstream of the RPL and Pilot stage exit, a short passage distance was added for better mixing. This is defined as mixing tube (pointed as location 'B' in Figure 3.3).

- The diverging Quarl section was made of Quartz (previously metal Quarl was used), which provided ample optical access of the flame zone (indicated as location 'C' in Figure 3.3).

- A flow conditioner device was added in the Main stage air flow path to get a uniform velocity profile before mixing (represented as location 'D' in Figure 3.3).

The experimental burner configuration used for the present thesis work is explained in Figure 3.3. The Pilot air stream flows through the series of impingement holes while cooling the RPL outer wall. The Main stage fuel supply pegs/rods are located between tangential swirl vanes (as shown in Figure 3.3 (b) and (c)).
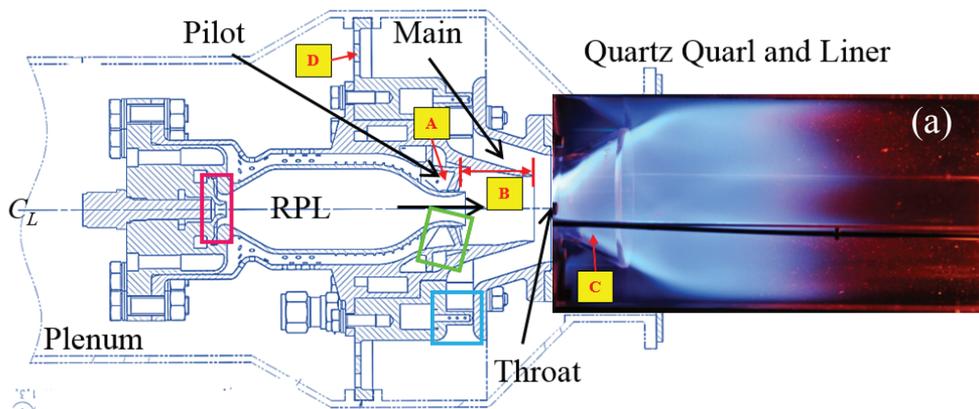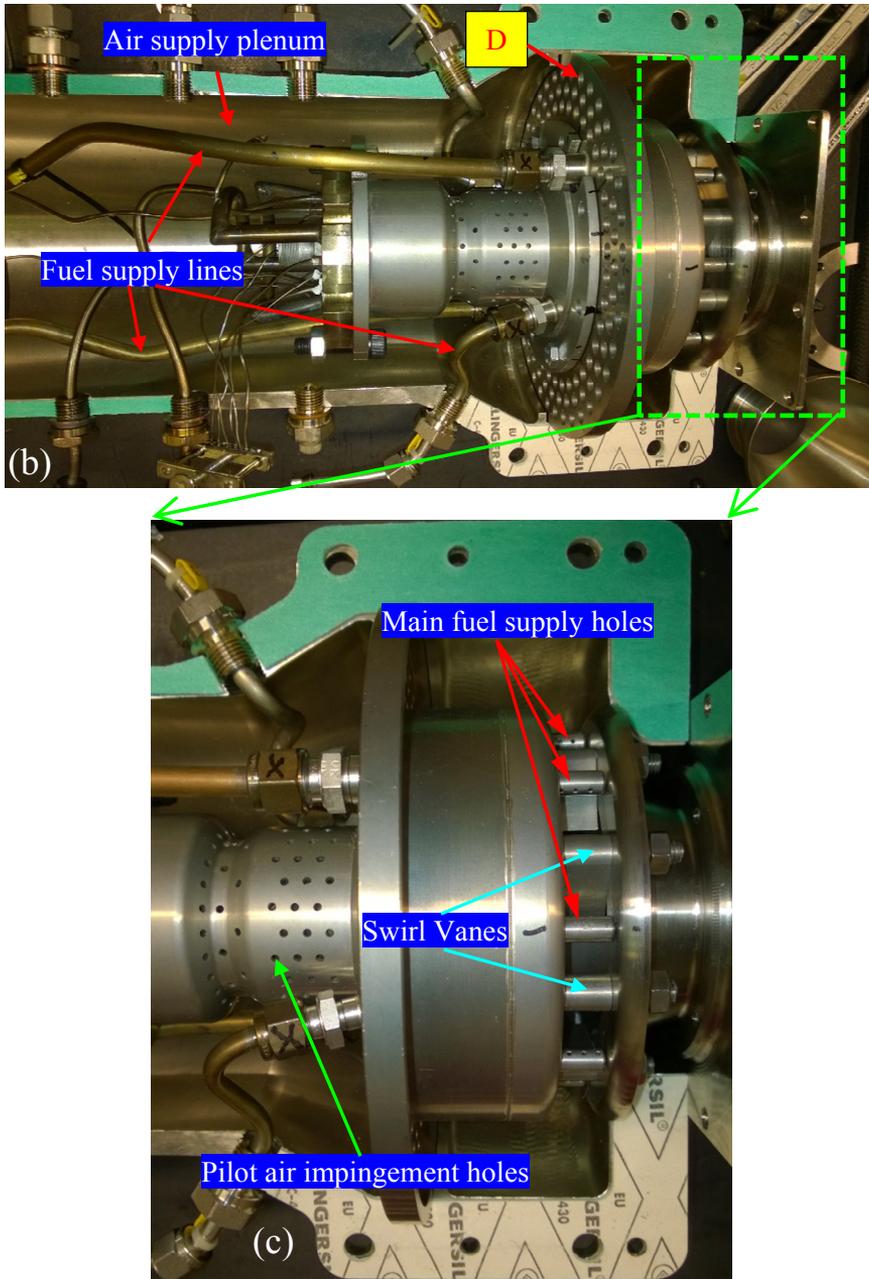
**Figure 3.3: Experimental downscaled DLE burner (Generation 2) for laboratory testing.**

Picture 3.3 (a) shows the burner cross section with liner arrangements. (b) indicates the actural hardware with air supply plenum and fuel supply line arrangements (c) shows the Main stage fuel air mixing devices (tangential vanes and the fuel injection rods with supply holes).

A common air plenum was used to supply air mass flow required for the Main and Pilot stages. The fuel air mixing locations are indicated in Figure 3.3 for respective burner stages: RPL (pink box), Pilot stage (Green box) and Main stage (Light blue box). All the fluid streams from the respective burner stage are merged at the burner throat location. Downstream of the throat location, a quartz made Quarl and liner zones were attached and acted as the combustor section. Figure 3.4 shows the burner stages and the mixing tube region from the exit direction.
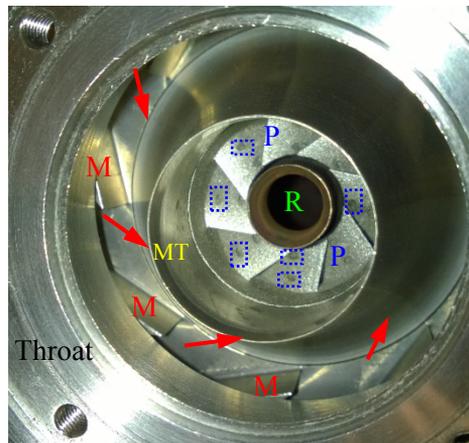


**Figure 3.4: The throat location of the experimental burner (view from burner exit).**

Burner Main stage tangential Swirl vane is indicated by 'M', the Main recatant flow path is indicated by the red arrows. Pilot stage axial swirl vanes with fuel injection holes (marked by blue recatangles) are indicated by 'P'. The RPL section is shown by 'R'. Mixing tube section is defined by 'MT'.

The Pilot stage was incorporated with axial swirl vanes and Main stage used tangential swirl vanes as depicted in Figure 3.4. Hot gas and product stream from the RPL and the Pilot reactant mixed partially inside the mixing tube. The third stream, the Main stage reactant mixture was introduced downstream to the mixing tube region. All swirl devices (RPL, Pilot and Main stage) produced an anti-clockwise swirl flow when viewed from the burner exit direction.

A separate burner arrangement was used while performing the RPL stage experiment (Paper I and II). This experiment was conducted eliminating the Main and Pilot stages. To restrict over heating of the RPL combustor, a dummy Pilot stage annular passage was designed. The new air flow passage was similar to the Pilot air flow passage except for axial swirl vanes and fuel injection ports. Figure 3.5 illustrates the system and burner design for RPL combustor experiment. The RPL combustor was not modified and the same hardware was used for all other experiments in this thesis.

Figure 3.5: Burner and system setup for RPL stage experiment.

# 3.3 System and Accessories

For performing the atmospheric test, many auxiliary systems were operated simultaneously. Two variable frequency driven blower supplied the combustion air flow for Main and Pilot stage. Gas fuel bottles were used for all experiments without any fuel preheating. The air streams were preheated (using electrical heaters) based on the calculated operating condition. For each stage fuel and RPL combustor air flow supply, dedicated mass flow controllers were installed. The Main and Pilot stage air flow streams (after mass flow rate recording and preheating) were merged at the base of the plenum section. The air mass flow rate distribution was defined by the Main and Pilot stage flow path effective area. The flow split was determined by performing a pressure drop test (between the plenum and liner exit) of the burner at atmospheric condition. Air and fuel flow rates were controlled by an in-house LABVIEW program. Two different laser systems were utilized for OH-PLIF (a combination of Nd: YAG and Dye laser) and 2D-PIV (Nd: YAG laser system) diagnostics. Laser sheets were passed through the flame (middle plane) and the images were taken using perpendicularly placed cameras (ICCD). Figure 3.6 shows the components and instruments used for performing the experiments. The RPL combustion experiments were performed using a long liner (620 mm). The bottom part of the liner (square cross section) was made of quartz for optical access. Another 315 mm long quartz made liner was used for all other experiments. Later for some experiments the square cross section liner was replaced with a circular cross section to investigate the influence of combustor aerodynamic on flame.

**Figure 3.6: Atmospheric test facility (instrumentation and layout).**

Total air mass flow rate was calculated so that it produced 60 m/s velocity at the throat location (considering 400 °C and bulk flow). The burner throat velocity was varied to 80 m/s for investigating higher pressure drop and load conditions. The global equivalence ratio ($\Phi_{Global}$) was varied from lean to rich stoichiometry ( down to LBO). The Main, Pilot and RPL stage fuel flow rates were varied to estimate the burner operability and emission performance. The RPL throat velocity (residence time changed) was varied by adjusting the total mass flow through the primary combustion zone. A spark plug (located at the RPL upstream center) was used to ignite the combustion process inside the RPL. Later Pilot and Main stage fuel flow was added to light up the Secondary flame. A water cooled multi holed emission probe was placed near the exit of the liner. The gas sampling was performed by extracting the hot combustion product gas from multiple location to reduce the spatial biasness. The equivalence ratios (and adiabatic flame temperatures) presented in this thesis were calculated from the sampled oxygen concentration (the confidence was within ± 2 %) [54].

# CHAPTER 4: MEASUREMENT AND SIMULATION TECHNIQUES

This thesis chapter presents the measurement techniques and simulation procedures. Along with conventional measurements (thermocouple and emission), advanced optical diagnostics techniques were applied. The optical techniques (Chemiluminescence, OH-PLIF and PIV) are described in this chapter. Then the CFD simulation method using ANSYS FLUENT is presented. A short description of CRN modelling (considering conceptual 1D heat transfer modelling) is explained in the last section.

## 4.1 Flame Chemiluminescence

Naturally, a flame can emit radiation in the following conditions [55].

- Black body radiation from soot or high carbon content particles (mainly found in diffusion type flames).

- At high temperature from rotation-emission bands, radiative heat transfer (due to $H_2O$ and $CO_2$ radiation from a particle free flames).

- Radiation emitted from atoms, molecules, or radicals, returning from an electronically excited state to ground state. This is generally known as Chemiluminescence.

Chemiluminescence naturally emits ultraviolet and visible radiation of flames, produced by short lived electronically excited intermediate species such as OH*, CH* or $C_2$*, which are formed during chemical conversion/reaction process in the thin reaction zone. The pre-fix "Chemi" specifies that the excitation energy originates from a chemical reaction energy sources. Flame Chemiluminescence can provide local heat release rate and equivalence ratio distribution [56]. It is reported that Chemiluminescence intensity has a linear dependency with fuel flow rate and the signal intensity drops exponentially with reduction of equivalence ratios. The Chemiluminescence intensity can be affected by local turbulence, flow properties

(strain) and fuel-air mixedness [57]. Figure 4.1 shows the Chemiluminescence spectrum for a methane-air and a hydrogen-air flame at atmospheric condition.
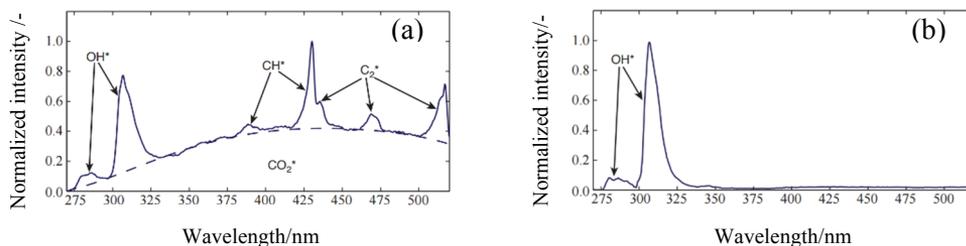


Figure 4.1: Chemiluminescence spectrum from flame.

a) methane-air b) hydrogen air flame at atmospheric pressure [58].

The emission spectrum is a superposition of the emissions from electronically excited species (OH*, CH*, $C_2$* and $CO_2$*). Narrow spectral band is visible from diatomic molecules, whereas $CO_2$* emits a broadband signal. A strong OH* signal around 300 nm to 330 nm can be observed from methane and hydrogen flames. Cheng et al. suggested that a strong correlation exists between the Chemiluminescence intensity ratio and equivalence ratio [59]. The presence of OH* peak at lean flame was observed from laminar flame experiment. In this thesis work, methane and hydrogen blended methane fuel experiments were conducted. As the burner operating conditions were dominantly in the lean regime (local unmixedness can produce partially premixed or diffusion type flames), the choice of OH* Chemiluminescence measurement was best suited for the prototype DLE burner experiments. A band pass filter was used to suppress other lights and the signal collection time was 100 μs. The Chemiluminescence signal was collected using a 10 Hz low speed and a 4.7 kHz high speed ICCD camera. The high speed ICCD camera recorded temporally resolved Chemiluminescence images, which were used to analyze the flame dynamics (applying FFT and POD). A major drawback with this technique is that it is a line-of-sight technique. The local 2D structure was not revealed, whereas an integrated signal (over the flame volume) was captured. In real gas turbine combustion system (Figure 4.2), flame sensors collect the UV Chemiluminescence emission to track the flame dynamics and its position.
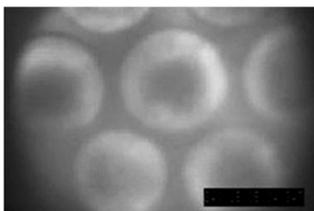


Figure 4.2: Water cooled CCD captured flame Chemiluminescence inside gas turbine combustor [60].

56

## 4.2 Laser Induced Fluorescence

Laser induced fluorescence is a diagnostic technique to capture spontaneous emission of the excited molecules/atoms when they are relaxed from higher energy band. It is a linear technique and mostly used in the visible and ultraviolet spectral regimes. Normally the process involves a Nd:YAG and a Dye laser system (Rhodamine 590 Dye was used for experiments). A tuned (specific frequency) laser excites the targeted molecules. The absorbed laser energy is indicated as process 'a' in Figure 4.3.
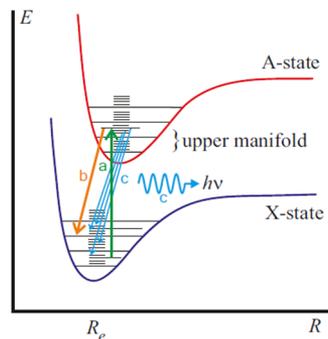


Figure 4.3: Electronic structure and LIF process [61].

As a result, laser energy moves the molecules from lower energy state (X-state) to higher energy level (A-state). The energized molecules stay in the A-state for some time. At the same time, energy is re-distributed across the other vibrational rotational levels in the A-state (defined as "upper manifold"). The energy can also be dissipated non-radiatively to a molecule during a collision (called "quenching") as shown in process 'b' (Figure 4.3). The remaining energy in the upper manifold (occupying many ro-vibrational levels) can relax back to the ground state (X-state) by releasing fluorescence photon from many transition (depicted as process 'c' in Figure 4.3). The fluorescence spectrum (non-resonant) differs from Rayleigh signal and can be captured by ICCD cameras. The local quenching is a serious problem for PLIF measurement. It depends upon the collision rate (a function of temperature) and the collision partners (species concentrations). In a gas turbine turbulent flame environment, it is very difficult to know all of the local quenching partner concentrations. The best possible solution is to perform the experiment with saturated fluorescence, where high laser intensity dominates over the spontaneous and quenching rate. The OH planar LIF measurement was conducted by expanding the laser beam (produced from Dye laser 283 nm) using a cylindrical lens (-40 mm). Later the laser sheet was collimated (focusing horizontal direction) using a spherical lens (+500 mm). The maximum laser power was focused on the flame measurement

region. An ICCD camera, fitted with UV sensitive lens (UV-Nikkor, f/4.5, f = 105 mm) was placed in perpendicular direction to the laser sheet. The simplified schematic shows the OH-PLIF measurement setup in Figure 4.4. A combination of a UG11 filter and a WG305 long pass filter were used in front of the camera to suppress scattering interference from the laser light and background radiation.
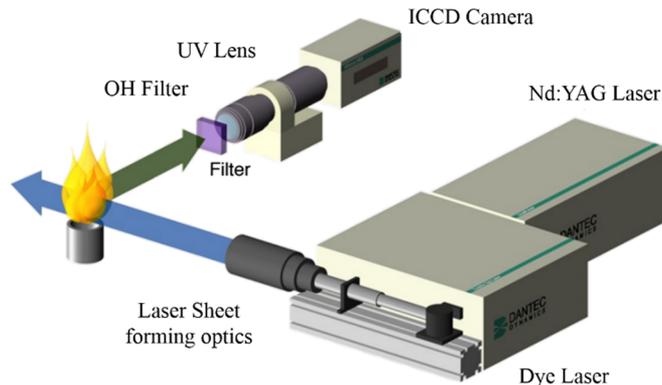


Figure 4.4: Simplified schematic of 2D PLIF measurement setup (Source: TUM).

The OH radical concentration was represented by the OH-PLIF images. The high intensity regions were believed to be the approximate flame front location (local temperature was greater than 1500 K), where superequilibrium amount of OH radicals were detected. The low signal intensity region indicated the post flame zones and convected OH concentrations. Overall, the OH-PLIF measurement provided a qualitative information of the flame and post flame zone. Quantification of OH concentration could be possible considering all energy transfer processes and quenching event.

# 4.3 Particle Image Velocimetry

Fundamentally, the gas turbine premixed combustion process depends on turbulent flame speed and flow velocity. The local and global flame structures, stability and flame anchoring processed are highly dependent on the flow field. Therefore, a detail understanding and accurate vector field measurement was essential. Particle image velocimetry technique is valuable for measuring the flow field vectors in reacting and non-reacting condition. Fluid motion and local turbulence can be captured using a seeded flow and PIV laser. It is a non-intrusive diagnostic technique, however seeding particle size can influence the flow if not selected

meticulously. Ideally the seeding particle should follow the flow without any alteration. The PIV measurement in a reacting flow could face challenges from flame, acceleration from gas expansion and non-uniform refractive index. Accumulation of seeding particle near wall and light scattering shows high level of data collection uncertainty. The technique is widely used for measuring 2D and 3D vector fields [62-64].
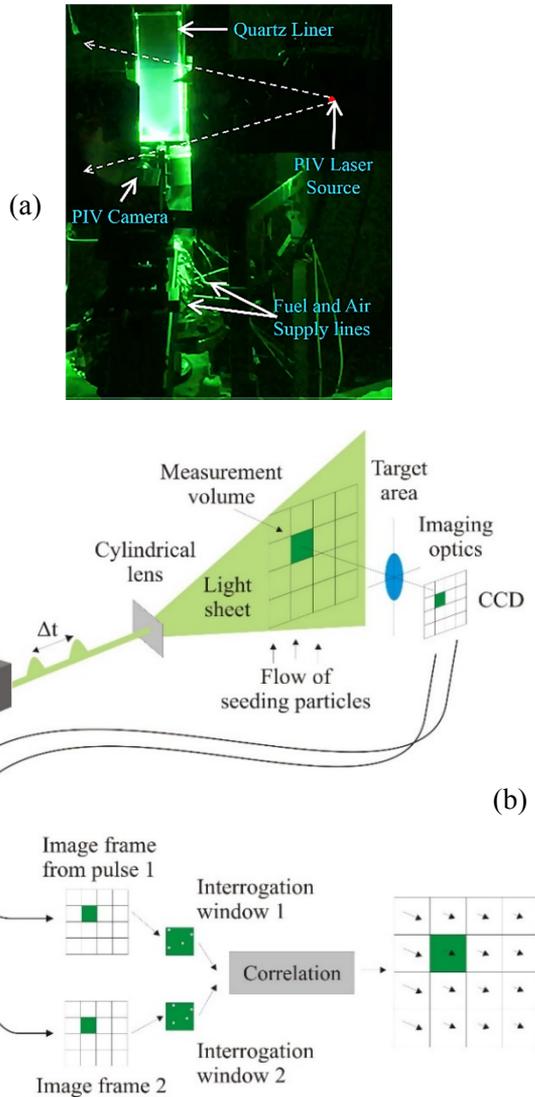


**Figure 4.5: Particle image velocimetry experiment.**

(a) Laboratory setup for PIV measurement (b) PIV working principle [65].

The basic PIV measurement principle depends on the accurate measurement of particle displacement and time. The rate of change of displacement predicted the velocity. The PIV measurement setup was used for the present experiment is shown in Figure 4.5 (a). Working principle of PIV is explained in Figure 4.5 (b).

In the atmospheric test facility, a PIV laser sheet was produced by Quantel double-pulse Nd: YAG laser and directed through the combustor mid plane (longitudinal direction as shown in Figure 4.5 (a)). Perpendicular to the laser sheet, a PIV image grabbing camera was placed. According to the PIV measurement principle, two laser sheets were produced by the double pulsed laser system. The PIV camera recorded image pairs (frame 1 and 2) for the double pulsed laser. The data was saved in the computer memory for post processing. The images were divided into small disjoint or overlapping interrogation windows. To compute the particle displacement, statistical approach was applied. Instead of tracking individual particles, the corresponding interrogation window pairs were cross-correlated. The spatial displacement that produced the maximum cross-correlation, statistically approximated the average displacement of seeding particles in the interrogation window. Thereafter, velocity associated with each interrogation window was calculated dividing the measured displacement with the laser pulse time delay.

Some special care was taken while deciding the seeding particle and seeding flow. The PIV signal intensity (Mie scattering) can increase with larger seeding particle diameter. But larger seeding particle often fails to follow the exact fluid flow. The seeding particle selection rule was followed to encounter this problem. It is recommended that for flow visualization, Stokes number should be less than 0.05 [66]. The seeding particle used for the experiments was $TiO_2$ (the Stokes number was < 0.05 [67]). The criteria for the seeding particles ($TiO_2$) to follow the flow, with an error of <1 % is ST<<1 [68, 69].
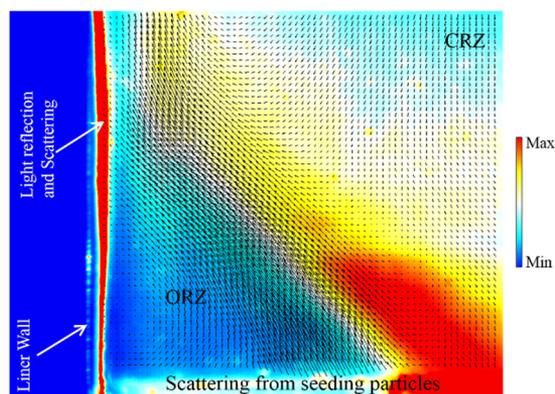


Figure 4.6: Flame image (Chemiluminescence) superimposed with the vector field.

The PIV measurement was performed downstream of the burner throat location. The flow field investigations were conducted for "with Quarl" and "without Quarl" configurations. Seeding particle buildup near liner and Quarl wall created light scattering problem and limited number of images were grabbed for reacting condition. Figure 4.6 shows that light scattering problem from the liner upstream and side walls.

# 4.4 Computational Fluid Dynamics Modelling

Numerical computation was performed for the prototype SGT-750 burner. Full 360° geometry of the burner was used for simulation. The cleaned burner geometry file was provided by Siemens. Later based on project requirement the geometry was modified. The studies were performed using commercial simulation tool ANSYS FLUENT [70]. These computations were performed to estimate pretest prediction and understand the experimental results (flow field and scalar distribution related). The simulation results were compared with the experimental results. The presented CFD simulations were the preliminary studies and should be considered as a crude approach for model validation. Further investigations (mesh sensitivity, effects of turbulence and combustion model, realistic boundary condition and non-adiabatic wall) could be performed for an optimized and accurate model validation.

### .4.4.1 Grid Generation and Operating Conditions

A tetrahedral mesh was generated using ANSYS ICEMCFD meshing tool. To reduce the computation cost without losing computational accuracy tetrahedral mesh was converted to polyhedral mesh in FLUENT. The benefits of polyhedral mesh are reported in literatures. This type of mesh show much lower cell count and comparable accuracy compared to tetrahedral mesh. Polyhedral mesh usually shows superior orthogonal quality and similar gradients as hexahedral mesh [71, 72]. The burner geometry (computational domain) is illustrated in Figure 4.7.
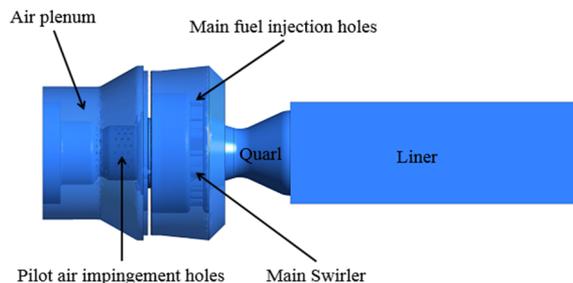


**Figure 4.7: Computational domain for lab scale DLE burner.**

Inside the RPL, mixing tube, fuel holes, swirl vanes and Quarl region, mesh densities were very high (maximum cell size was 0.5 mm). For RANS and SAS simulation 14 million polyhedral grid was used. Later for performing LES, a 22 million refined grid was generated. The liner length was kept similar to the experimental setup. The simulations were performed at atmospheric condition with preheated air (400 °C). Mass flow rate boundary conditions were applied for all fuel and air inlets. The air mass flow rate split (between Main and Pilot stage) showed 2 % variation when compared with the experimental results. A pressure outlet boundary condition was applied at the burner exit. All the walls were considered as adiabatic rigid wall. However, for Paper I, RPL wall thickness was modeled and a simplified conjugate heat transfer computation was performed. The computational domain is described in Paper I. The default solver settings of ANSYS FLUENT were used for numerical analysis. Turbulence and combustion models were used based on ANSYS FLUENT recommended best practices, theory and user guides [73, 74]. The highly turbulent reacting CFD simulation require mass, momentum, energy and species conservation equations to be solved on the entire grid [31, 75]. Following section describes the brief explanation of the modelling techniques used for the simulation.

## 4.4.2 Turbulence Modelling

Flow field inside the DLE burner was turbulent (Re > 45000 based on bulk flow at throat and iso-thermal condition). The local velocity fluctuations were normally generated by the swirl component, shear layer, velocity gradient and the combustion process. As a result, the turbulent flow was associated with multiple length and time scales. Three dimensional rotating structures, called eddies were produced inside the swirling turbulent flow domain. The largest eddy size was equal to the integral length scale (can be assumed as the burner throat diameter or the liner diameter). Large eddies were unstable and broke up into smaller eddies and the kinetic energy was transferred to smaller eddies. This process was repeated several times and transfer the kinetic energy continuously to smaller scale eddies (Kolmogorov length scale). At this point, the kinetic energy of Kolmogorov length eddies can be dissipated by molecular viscosity. Generally, flow associated with the large scale eddies are anisotropic and their structure is determined by the combustor flow field/boundary conditions. However, the small scale turbulent motions are isotropic and the statistics of this small scale turbulent motion can have a universal form. The energy cascade process in turbulent flow is shown in Figure 4.8. Direct numerical simulation can solve the whole energy spectra from integral length to Kolmogorov scale but it is computationally expensive and not suitable for industrial application.
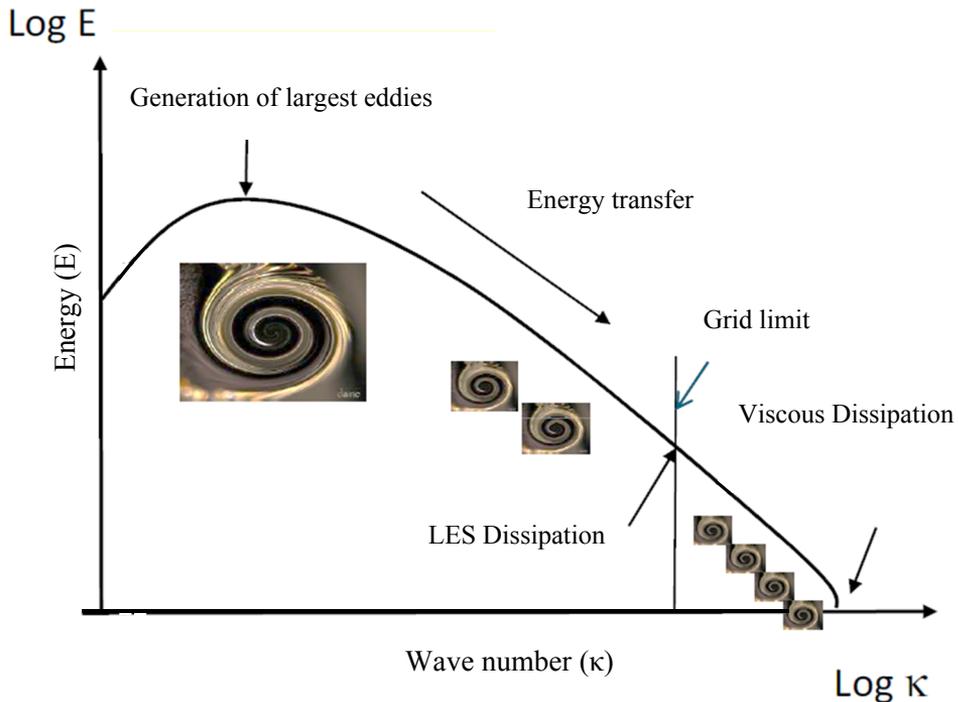
Figure 4.8: Energy cascade and eddy size in turbulent flow (Source: ANSYS).

In RANS approach, an additional Reynolds stress term appear while performing averaging of the momentum equation as an effect of turbulence. To close the equation, Reynolds stress term was modeled using $\kappa - \varepsilon$ turbulence model [75]. A modified version of $\kappa - \varepsilon$ model called Realizable $\kappa - \varepsilon$ model was used for RANS calculation. The major difference of this model with the original is the different formulation of turbulent viscosity. This model is widely used in industry and can capture strong streamline curvature, vortices, and rotational flow structures [74]. The model captured the mean flow field but failed to calculate the unsteady nature of the flame.

Initially, the unsteady simulation was performed using an improved URANS approach. The SAS modelling concept is based on the introduction of the von Kármán length-scale into the turbulence scale equation. The information provided by the von Kármán length-scale allows SAS models to dynamically adjust to resolved structures in a URANS simulation, as a results an LES-like behavior in unsteady regions of the flow field was achieved. The model provided standard RANS capabilities in stable flow regions. The detail of this model can be found literature [76].

Finally, an advanced unsteady simulation was conducted following large eddy simulation approach. The grid size was refined to resolve at least 80 % of the turbulent kinetic energy. The general idea of LES is the governing equations are obtained by filtering the time-dependent Navier-Stokes equations in either Fourier (wave-number) space or configuration (physical) space. The filtering process effectively filters out eddies whose scales are smaller than the filter width or grid size used in the computational domain. The resulting equations therefore govern the dynamics of large scale eddies. Figure 4.8 shows that grid limit for LES computation. Under the grid limit, subgrid scale modeling approach was considered. In ANSYS FLUENT the finite-volume discretization process itself implicitly provides the filtering operation. Sub grid scale stress tensor term was modeled as Boussinesq hypothesis. The turbulent viscosity was calculated using Dynamic Kinetic Energy Subgrid-Scale Model. According to the theory, the subgrid-scale turbulence was better modeled when the transport of the subgrid-scale turbulence kinetic energy was considered. More detailed about the LES approach could be found in ANSYS FLUENT theory and User guide [73, 74].

## 4.4.3 Combustion Models

The combustion process inside the DLE burner is assumed to be partially premixed. The mixing time for Pilot fuel and air was limited; whereas adequate mixing time was provided for the Main stage. Therefore, non-uniform reactant mixture pockets can be found inside the burner. The partially premixed combustion model was used to encounter diffusion and premixed type of flames. This model is based on FLUENT non-premixed and premixed combustion model. Both non-premixed and premixed flame assumes that the combustion process occurs in thin laminar one dimensional flamelet structure. The flamelet can be wrinkled by the turbulent eddies but the inner structure was not modified. Steady diffusion flamelet model was used for steady RANS and unsteady SAS simulation using methane fuel. Hydrogen blended flames and LES simulations were performed using premixed FGM. Partially premixed combustion model solves mean reaction progress variable ($\bar{c}$), mean mixture fraction ($\bar{f}$) and mean mixture fraction variance ($\bar{f}'$) when laminar diffusion flamelet was used. One extra variable variance of reaction progress variable ($\bar{c}'$) was solved when premixed FGM was used. The Zimont turbulent flame speed model was used to close the mean reaction rate term in progress variable transport equation. On the other hand, non-premixed model mapped the scalar quantities in mixture fraction space. The scalar quantities (temperature and species mass fraction) were described by mixture fraction($\bar{f}$) and scalar dissipation ($\chi$) terms. Later the local scalar values were computed from the PDF of $\bar{f}$ and $\chi$. More detail about the models and guidelines can be found in ANSYS Theory guide [74].

The diffusion flamelet model (defined as LFM) and FGM both assumes that a turbulent flame is an ensemble of laminar flames. The laminar flame internal structure is not significantly altered by the turbulence. But the FGM combustion model is fundamentally different from the Laminar Flamelet model. Laminar Flamelet model are parameterized by strain, hence the thermochemistry always inclines toward chemical equilibrium (strain rate decays towards the outlet of the combustor). On the other hand, the FGM model is parameterized by reaction progress and the flame can be fully quenched (by excess dilution air). Hence the FGM model is better for ignition and extinction modeling.

# 4.5 Chemical Reactor Network Modelling

The CFD simulation is computationally heavy and require long time to converge. A simplified approach was selected to perform 1D calculation considering full chemistry. ANSYS CHEMKIN 1D tool was used for constructing the CRN model [77]. As the tool does not count for the fluid dynamics effect, flow information was collected from the steady state CFD calculation. Multiple PSR and PFR were used for the CRN modelling. Various chemical kinetic mechanisms were applied in the model to compare their effect on emission prediction. Heat loss reduces the flame temperature and reaction rates, which can drastically modify the flame pollutant formation. Volumetric heat loss data was included in the CRN calculation.

### 4.5.1 Gas Turbine Network Modelling

PSR is a theoretical reactor model which assumes perfect mixing inside the control volume. The mixing process inside the PSR is instant due to turbulent mixing. So any combustion process inside PSR control volume could be controlled by chemical reaction rate not by mixing time scale. A PSR model in CHEMKIN require a residence time for steady state simulation. The residence time can be calculated using the mass flow rate and the volume [78].

Another type of theoretical reactor was used for constructing the CRN model was PFR. The post flame zone was modeled using PFR. It is a duct/channel type 1D reactor, where temperature and composition can only vary in the axial direction (no gradient in radial direction).

As shown in Figure 4.9, gas turbine combustion can be modeled using the series of PSR and PFR. The mixing zone, flame zone and recirculation zones can be represented with PSR. The post flame zone provides the residence time for reaching equilibrium condition. The PFR reactor is critical for slow reacting species (i.e. NOx

formation and CO oxidation). For the DLE burner, the flame zone was modeled with a PSR and the residence time was defined as the chemical time scale. Recirculation flow and residence times were apprehended from CFD simulation. Detail description of the flow splits and residence time is described in Paper III and IV.
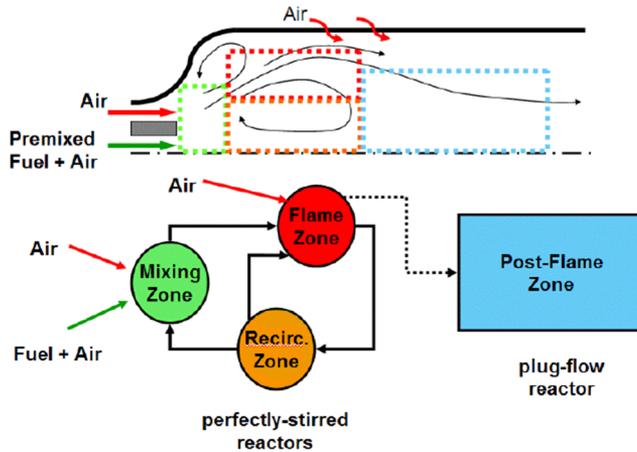


**Figure 4.9: Gas turbine network using PSR and PFR [77].**

## 4.5.2 Heat loss Modelling

Accurate heat loss calculation is essential for a quantitative realistic emission prediction. Local flame quenching, volumetric heat loss and near wall condition highly affects the CO and NOx formation. The heat loss calculation from the DLE combustion is a very complex process, which involves conduction, convection and radiation heat loss. The accurate heat loss prediction can be done using experiments and 3D CFD calculation. In this work, a simplified empirical method was used. Figure 4.10 shows the 1D heat loss model to calculate heat transfer from the RPL and liner [79].

The secondary flame heat loss was mainly dependent on convection and radiation. Hot gas flow along the liner (convection) and radiation from the $H_2O$ and $CO_2$ molecules (infrared heat radiation) were heating up the combustor. On the other side, liner was cooled by the outside ambient air convection (a suction device was used to remove the combustion gas through vent) and radiation. The conduction heat loss was comparatively small compared to the convection and radiation. In the model, $C_1$ and $C_2$ represented the convective heat flux from hot gas and cold ambient air. The radiative heat flux for hot gas and ambient air were $R_1$ and $R_2$ respectively. The conduction heat flux was defined by $K_{1-2}$.
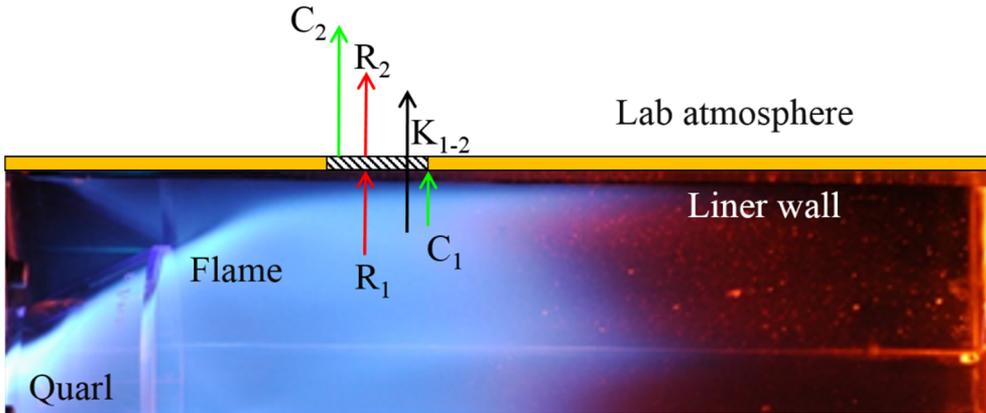
**Figure 4.10: One dimensional heat loss model.**

Subscript '1' indicate the hot flame region; whereas subscript '2' shows the ambient condition. Flow direction is from left to right.

At steady state condition, the heat flux was related to

$$R_1 + C_1 = R_2 + C_2 = K_{1\text{-}2}$$

Using the above formula and combustor inlet conditions of pressure, temperature, air mass flow rate, and air/fuel ratio, heat loss from the combustor was calculated [79]. The RPL heat loss was also estimated following the similar approach.

# CHAPTER 5: RESULTS AND SUMMARY OF PUBLICATIONS

## 5.1 Key Results

This section highlights some of the key findings from the experimental and numerical study which are included in the papers. Swirl flame stabilization and its structure is explained. Burner operability, LBO and Stage interaction results are described in this chapter. Effect of combustor aerodynamics and hydrogen blending with methane showed significant change in flame. Finally, results from PIV measurement results are included.

### 5.1.1 Flame stabilization

The primary flame was stabilized inside the RPL and the secondary flame was visualized from the Quarl and liner region. Two distinct flame regions can be understood from Figure 5.1.
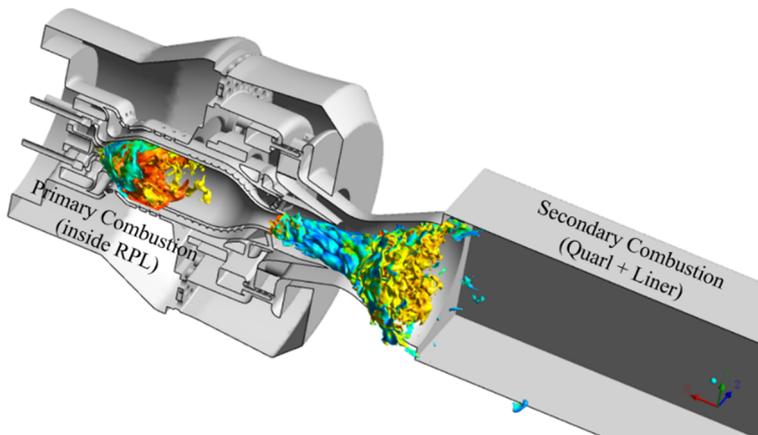


**Figure 5.1: Primary and Secondary flame location inside DLE combustion system.**

Flames are identified by the instantaneous OH concentration Iso-surface (primary and secondary flame).

Figure 5.1 indicates that the diverging geometrical locations were mainly responsible for flame anchoring in the primary and secondary flame region. A continuous flame was visible from RPL exit to the liner. This flame region (inside the mixing tube) was produced by the interaction of fresh reactant mixture (Pilot stage) with the hot RPL product stream. The combustion of Pilot and Main fuel was completed inside the liner. Inside the Quarl and liner, strong swirling reactant jet produced a low-speed region along the burner centerline, where vortex breakdown induced recirculation bubble was formed. The vortex breakdown process provided strong flame stabilization, and the mechanism involved (1) formation of a forward stagnation point and (2) recirculation of hot combustion product. The flame was stabilized along ISL, which was formed between CRZ and incoming reactant stream. The secondary flame was elongated downstream to the liner region as some fraction of Pilot and Main fuel-air mixture was combusted inside the liner. Figure 5.2 shows the total flame (secondary) macro structure and the stabilization points.
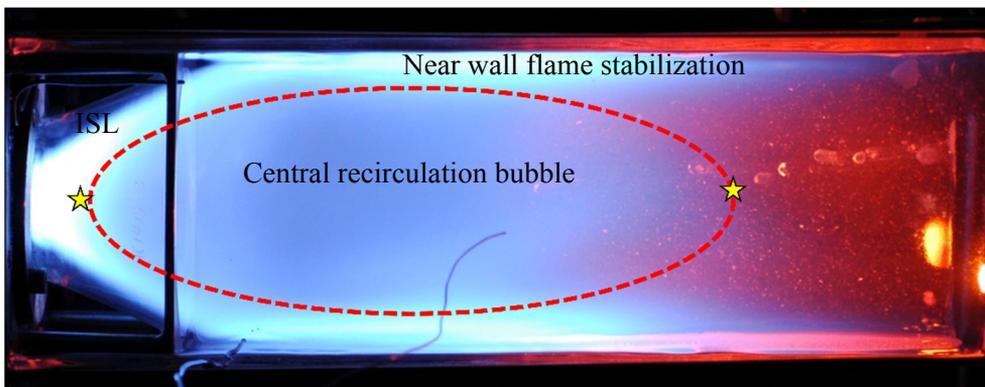


**Figure 5.2: Secondary flame macro structure inside liner and Quarl.**

Flow direction is from left to right. Stagnation points (forward and backward) are shown by the yellow stars [80].

Figure 5.3 explains the recirculation zone in detail. The Q-criterion iso-surface ($10^8$) is plotted around the CRZ (Figure 5.3) and colored by local tangential velocities. A strong vortex core was formed inside the RPL combustor and propagated downstream and merged with the main combustion zone. The rotating structures interacted with the Pilot and Main streams; hence local turbulent intensity was increased. Density and temperature gradients were present in the inner shear layer (mixing tube and Quarl region), where flame experienced high stretch rate and straining due to shear force. At the center, 3D rotating helical structure was appeared and indicated the approximate location of the processing vortex core (PVC) on the axially propagating vortex. The low pressure core was radially pulled away from the center line while travelling downstream. This process produced a spirally rotating motion of vortical structures surrounding the CRZ as shown in Figure 5.3.
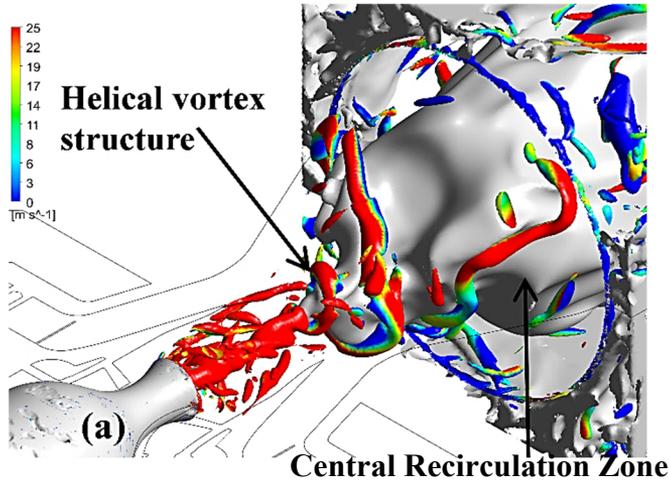
**Figure 5.3: Helical vortex structure around the central recirculation zone.**

Where (a) represent the RPL combustor and the flow is from left to right direction [80].

## 5.1.2 Burner Operability (NOx and CO Emission)

The primary combustion zone equivalence ratio was varied to explore the burner overall emission performance and operability. The NOx emission variation is explained in Figure 5.4 as function of flame temperature and RPL stoichiometry.
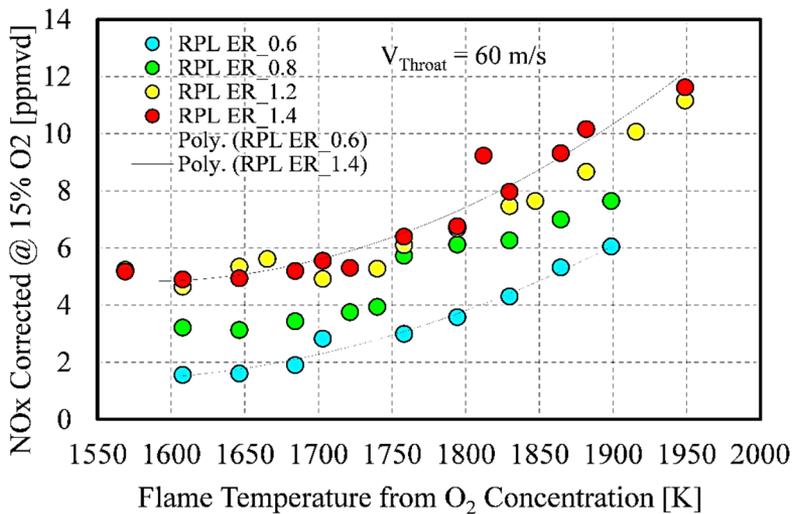


**Figure 5.4: Burner NOx emission as a function of flame temperature and RPL stoichiometry [38].**

The impact of RPL stoichiometry on NOx emission was noticed. The rich RPL combustion produced higher NOx and lean RPL showed a lower NOx emission. The RPL combustor showed strong effect on burner NOx performance. The exponential growth of NOx was observed when the flame temperature crossed 1750 K (Figure 5.4 shows the DLE burner NOx performance).

Figure 5.5 explains the LBO event, which was identified from the exponential growth of CO concentration. The high concentration of CO was found at very low flame temperature around 1600 K. At higher flame temperature, CO concentration was reduced (higher CO oxidation rate). At higher flame temperature (beyond 1900 K) dissociation of $CO_2$ to CO yielded an increase of CO concentration. Figure 5.5 also indicated LBO benefits while the burner was operated with rich RPL.
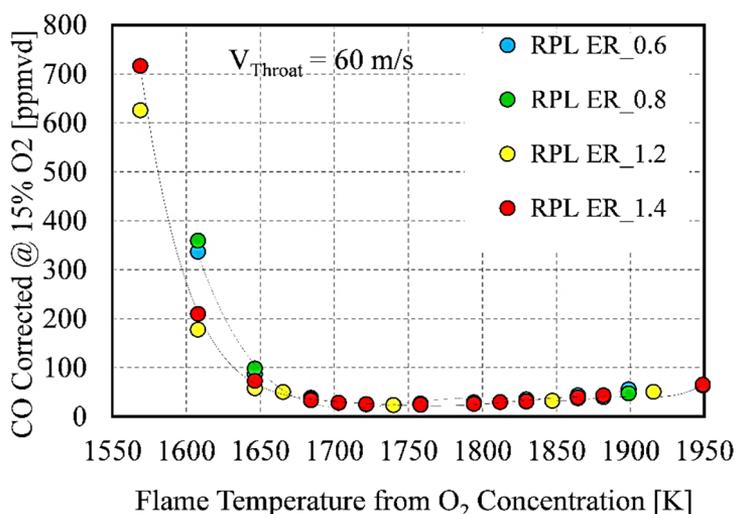


Figure 5.5: Burner CO concentration variation and LBO as a function of flame temperature and RPL stoichiometry [38].

## 5.1.3 Burner Stage Interaction

Pilot and RPL stage combustion showed great influence on burner combustion characteristic and emission. The detail results are explained in [80]. Figure 5.6 shows the combine effect of RPL stoichiometry, RPL residence time (by varying total air mass flow) and Pilot fuel % on burner total NOx emission. For all instances NOx emission was increased with the increase of Pilot fuel. Lean RPL showed NOx benefits but a non-liner dependency was observed around 1.2 RPL equivalence ratios. Higher RPL residence time (RPL_Res) reflected less NOx as the amount of fuel supply to the primary combustion zone was decreased. In total, RPL

stoichiometry and Pilot fuel flow showed strong interaction and dependency on burner NOx performance. A lean RPL and lean Pilot was preferable for NOx emission reduction. This can be achieved at base load condition. But at part load operation, stability might be affected.
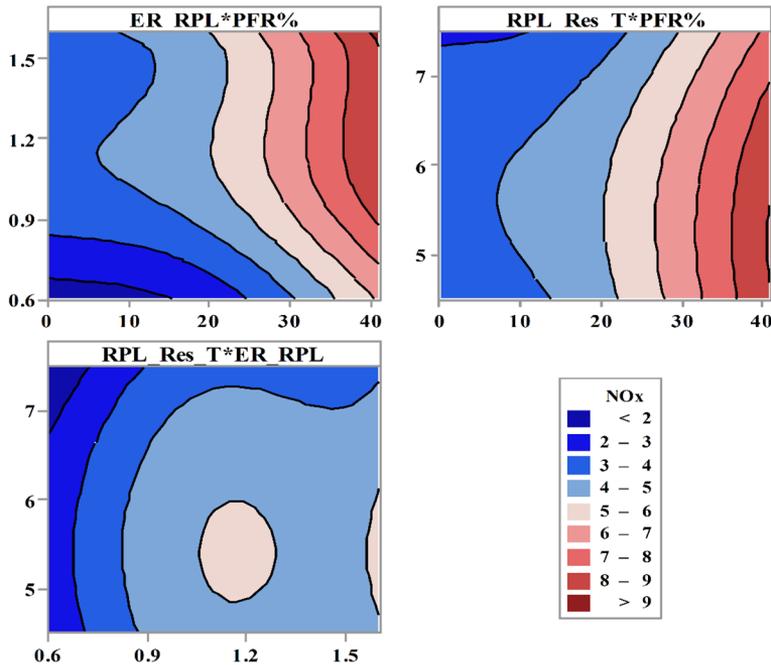


**Figure 5.6: Pilot-RPL interaction effect on NOx emission [80].**

## 5.1.4 Effect of Combustor Geometry

Gas turbine combustion process is highly sensitive to the burner and combustor geometry. The flame anchoring and stabilization location could be modified with a small geometrical/aerodynamic change. In this experiment, liner geometry was modified by eliminating the Quarl (diverging) flame stabilizing section. The OH-PLIF images are shown in Figure 5.7 indicates that without Quarl (defined as Dump), the flame shape was quite different than baseline (with Quarl) [37, 38]. The Quarl wall provided a boundary and flame was not able to radially expand. The radial expansion of the flame was noticed for Dump combustion case. The flame surface area was increased and the total flame length was reduced. Along with CRZ, another ORZ was formed. At higher equivalence ratio a semi-stable secondary flame was observed. The secondary flame intermittency caused flame instability and reduced the burner operating window in the high stoichiometry regime.
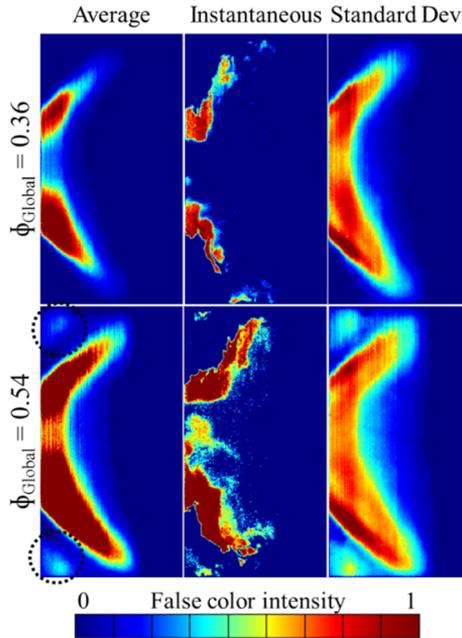
**Figure 5.7: Secondary flame formation in ORZ at rich stoichiometry.**

The ORZ region helped to recirculate the gas mixture and increased the flow residence time. The mixing process of reactant with recirculated hot product was increased due to ORZ. Oxidation of CO was also improved as shown in Figure 5.8. The Dump combustor showed better LBO capability and extended lean operation of the burner.
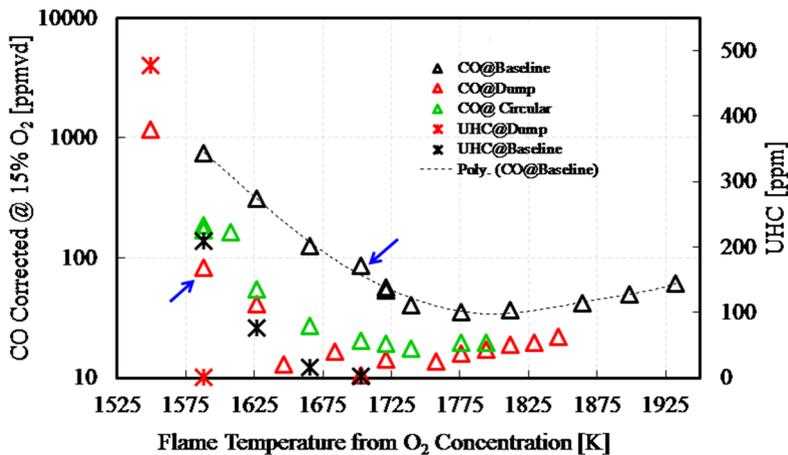


**Figure 5.8: Variation of CO concentration and LBO with flame temperature.**

## 5.1.5 Fuel Flexibility of the Burner

As discussed previously (Chapter 2), fuel flexibility of gas turbine combustion system has high impact on efficiency, operability and emission performance. The DLE burner fuel flexibility was tested by introducing new type of fuels. Hydrogen (up to 50 % by volume) blended flame showed significant change in burner operability and flame structure. By adding hydrogen, thermo-chemical properties were modified and turbulent flame speed was increased. High diffusivity and higher flame speed of hydrogen molecule reduced the total flame length. Another important observation was the extension of lean operating limit for hydrogen flame. Figure 5.9 illustrates the LBO extension of the burner by adding hydrogen.
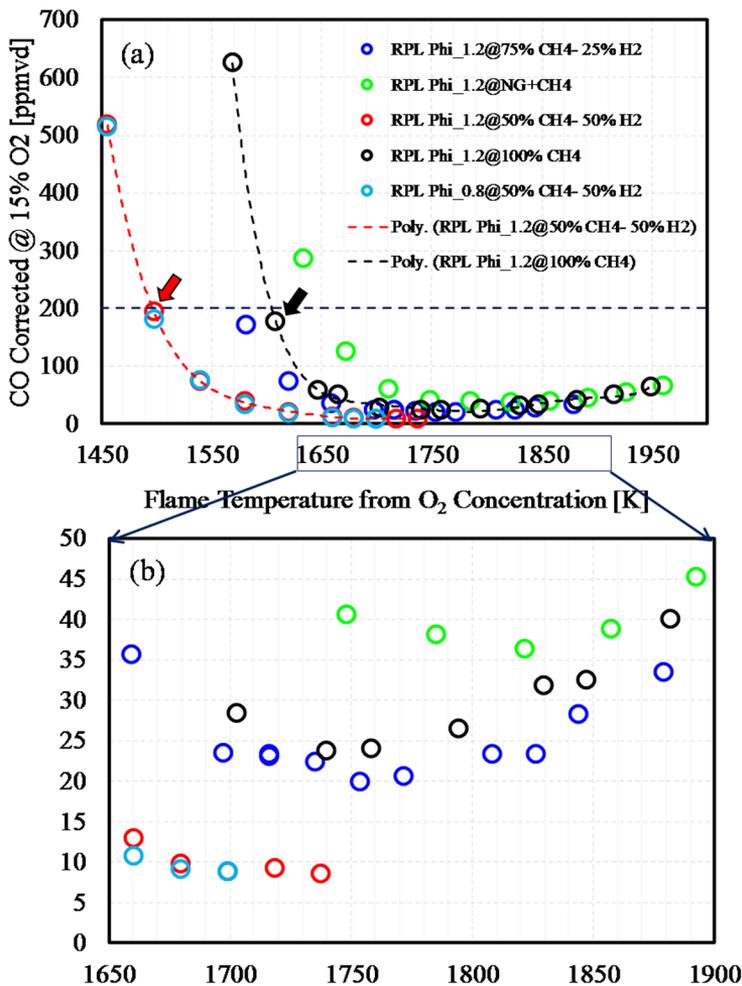


Figure 5.9: Variation of LBO and CO concentration with different fuel.

## 5.1.6 Flow Characteristics

PIV measurement was performed to investigate the reacting and non-reacting flow field. The reacting flow measurement suffered serious problem of light scattering and seeding particle accumulation near the wall (upstream and side walls). Hence, the statistics were determined from limited measurements. Both reacting and non-reacting flow PIV measurements captured the main features (the CRZ, ISL, ORZ and the high velocity annular jet) qualitatively. An expanding CRZ (in radial direction) was noticed compared to the non-reacting case. Figure 5.10 shows the measured velocity and turbulence field for reacting and non-reacting flow. Detailed PIV measurement results are included in Paper XI.
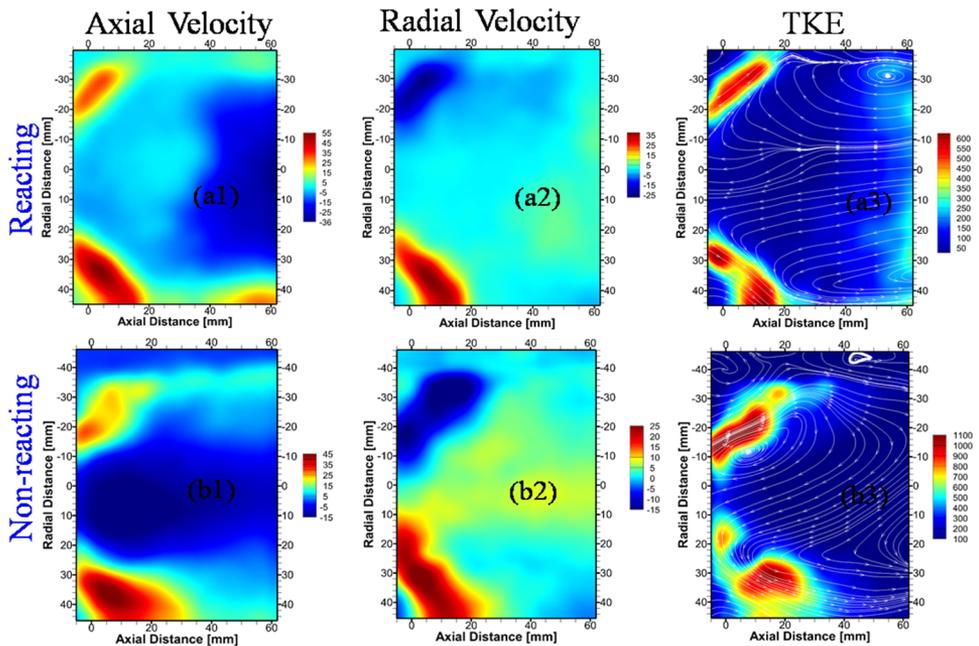


**Figure 5.10: Flow field measured by the PIV experiment.**

Flowfield comparison of reacting (picture a1, a2 and a3) and non-reacting case (picture b1, b2 and b3). Detailed reuslts are included in Paper XI.

# 5.2 Summary of Publications

**Paper I:**

*Operability and Performance of Central (Pilot) Stage of an Industrial Prototype Burner*

By Atanu Kundu, Jens Klingmann, Ronald Whiddon, Arman Ahamed Subash and Robert Collin

ASME 2015 Power Conference: POWER2015-49449

This paper was focused on the operability investigation of central stage of the DLE 4th Generation burner at atmospheric condition. The central stage was called "Rich-Pilot-Lean" or RPL. The RPL stage was critical for swirl stabilized flame for preventing any discontinuity of flame during various load condition. It supplied heat and radicals to the forward stagnation point of the main flame region and an uninterrupted combustion process was established. The RPL combustion was analyzed by varying the equivalence ratios and co-flow air temperature. Emission, flame location and operability were measured. At the RPL exit, OH radicals and partially combusted product concentrations were visualized using Chemiluminescence Imaging. A simple PSR based chemical kinetics calculation and RANS CFD (considering heat transfer process through the RPL wall) analysis were conducted for the RPL combustor.

*I have actively participated in the test campaign and supported with hardware modification and setting up the experimental arrangement. Helped my coworkers for performing experiments and recording flame images. I was mainly responsible for emission measurement and recording Chemiluminescence images. Whereas, A. A. Subash and R. Whiddon were mainly responsible for setting up optical measurement system, defining operating conditions and post processing of Chemiluminescence images. I have post processed the emission data and performed CFD and chemical kinetics analysis. As a lead author, I wrote the paper with the experimental results and post processed results from CFD and chemical kinetics study. R. Collin and J. Klingmann supervised the experiment and writing.*

**Paper II:**

*Flame Investigation of a Gas Turbine Central Pilot Body Burner at Atmospheric Pressure Conditions Using OH PLIF and High-Speed Flame Chemiluminescence Imaging*

By Arman Ahamed Subash, Ronald Whiddon, Robert Collin, Marcus Aldén, Atanu Kundu and Jens Klingmann.

ASME 2015 Gas Turbine India Conference: GTINDIA2015-1212

This paper was based on the previous experiment (Paper I) and mainly focused on optical diagnostics results. High speed Chemiluminescence and OH-PLIF images were collected from the RPL exit location. The variation of RPL equivalence ratio affected the flame shape and its structure. The RPL co-flow temperature and flowrate also altered the flame stabilization. The flame dynamics was captured by the high speed Chemiluminescence imaging. Proper Orthogonal Decomposition tool was applied on the time resolved Chemiluminescence images to determine the flame oscillation frequency and mechanisms. The NOx measurement was also performed to complement the measurement for different operating conditions.

*As a Co-author, my contribution to this paper was to perform experiment and assist A. A. Subash and R. Whiddon for performing OH-PLIF and Chemiluminescence measurement. R. Whiddon was responsible for setting up/deciding operating conditions. A. A. Subash post processed the OH-PLIF and Chemiluminescence images. I have post processed the NOx emission data and actively participated in the technical discussions for writing the paper. M. Alden, R. Collin and J. Klingmann supervised the experiment and writing.*

## Paper III:

*Flame Stabilization and Emission Characteristics of a Prototype Gas Turbine Burner at Atmospheric Conditions*

By Atanu Kundu, Jens Klingmann, Arman Ahamed Subash and Robert Collin

ASME Turbo Expo 2016: GT2016-57336

The 4th generation prototype SGT-750 burner was investigated experimentally in atmospheric condition. The primary purpose of the research was to explore the flame stability, operability and emission capability of the new conceptual burner. OH Planar Laser-Induced Fluorescence (OH-PLIF), and Chemiluminescence imaging were performed to characterize the flame structure and location. NOx, CO and UHC emissions were measured using a water-cooled emission probe. Different instability points (lean operation and burner staging influence) were identified and global flame operability window enhancement possibilities were explored. Numerical analysis was carried out using FLUENT to understand the scalar and vector fields. Simplified chemical reactor network model was also developed to compare the measured emission data with model.

## Paper IV:

*Pilot-Pilot Interaction Effects on a Prototype DLE Gas Turbine Burner Combustion*

By Atanu Kundu, Jens Klingmann, Arman Ahamed Subash and Robert Collin

ASME Turbo Expo 2016: GT2016-57338

This paper was based on experimental investigation on Pilot flames (the RPL and Pilot stage), their interaction and influence on "Main" flame stability. The RPL flame residence time, equivalence ratios were varied, whereas Pilot fuel ratio was also varied to experimentally establish a correlation between Pilot flames contribution on "Main" flame operability. Flame imagining (PLIF and Chemiluminescence), emission measurement and numerical analysis (CFD and Chemical kinetics) were performed. Statistical method was employed to understand the results scientifically.

## Paper V:

*Laser-Based Investigation on a Dry Low Emission Industrial Prototype Burner at Atmospheric Pressure Conditions*

By Arman Ahamed Subash, Robert Collin, Marcus Aldén, Atanu Kundu and Jens Klingmann

ASME Turbo Expo 2016: GT2016-57242

This paper was based on detailed laser diagnostics investigation on the DLE burner flame. Flame macro structure and local characteristics were visualized with OH-PLIF and Chemiluminescence imaging. Stage wise (RPL, Pilot and Main) contribution of the secondary flame was analyzed in detail. Flame stabilization, shape and its fluctuation were quantified with the help of OH-PLIF and

Chemiluminescence images. The overall flame structure and its influence on global flame emission was measured for different operating conditions.

*I have planned the experiment and decided the operating points/test schemes. A. A. Subash was responsible for performing OH-PLIF experiment and post processing of LIF and Chemiluminescence data. Whereas NOx emission data was post processed by myself. I have assisted A. A. Subash for performing optical measurements and interpreting the experimental results. R. Collin and J. Klingmann supervised the experiment and paper writing.*

## Paper VI:

*Experimental and Numerical Investigation of a Prototype Low NOx Gas Turbine Burner*

By Atanu Kundu, Jens Klingmann, Arman Ahamed Subash and Robert Collin

ASME 2016 PowerEnergy Conference: PowerEnergy2016-59592

Main objective of this paper was to investigate flame stabilization process with the help of experimental results and numerical analysis. CFD simulation was performed by ANSYS FLUENT. The CFD simulation results helped to understand the underlying physics behind the flame stabilization process and burner staging concept. Chemical kinetics calculation results were compared with CFD and experimental data.

*I am the lead author for this paper and performed the experiments with help of A. A. Subash. Test planning, selecting operating points and construction of experimental setup was done by me. Besides that, I have performed numerical analysis (CFD and Kinetics) and post processing. A. A. Subash has done the OH-PLIF, Chemiluminescence (I have also assisted) measurements and post processing of OH-LIF images. R. Collin and J. Klingmann supervised the experiment and paper writing.*

## Paper VII:

*Impact of Combustion Chamber Geometry on a Partially Premixed Swirl Flame*

By Atanu Kundu, Jens Klingmann, Arman Ahamed Subash and Robert Collin

ASME Turbo Expo 2017: GT2017-64677

In this paper, combustor/liner cross sectional geometry modification was performed to investigate the influence of aerodynamic change on the flame macro structure. Detailed measurements were performed using Methane fuel. The Geometrical modification includes, (1) removal of the diverging Quarl section (this was integral part of the combustion system for paper III, IV, V and VI) (2) change the square cross section liner with circular cross section. Optical measurements with OH-PLIF, PIV and Chemiluminescence were performed for wide ranges of operating conditions. Detailed emission measurements and numerical analysis (CFD

modelling using FLUENT) were carried out. The results (emission and flame stabilization process) were compared with previous "with Quarl (Baseline)" arrangement. The 2D PIV measurement provided flow filed information and the results were compared with CFD simulation results. The flame stability and operability were characterized using CO emission and Chemiluminescence images.

*I led the experimental campaign by planning, calculating and selecting operating conditions. Any rig specific modifications (hardware and software) were resolved by myself and A. A. Subash. I was responsible for emission measurement, Chemiluminescence image acquisition (with help of A. A. Subash) and post processing results. OH-PLIF measurement, post processing and still picture acquisition were performed by A. A. Subash. I have also performed the numerical calculation, setting up PIV experiment (with the help of A. A. Subash) and performed PIV results post processing; whereas R. Collin and J. Klingmann supervised the experiment and paper writing.*

## Paper VIII:

*Fuel Flexibility of a Multi Staged Prototype Gas Turbine Burner*

By Atanu Kundu, Jens Klingmann, Arman Ahamed Subash and Robert Collin

ASME Turbo Expo 2017: GT2017- 64782

This paper was based on fuel flexible capability estimation of the prototype burner. Hydrogen was added with methane up to 50 % by volume and natural gas for these experiments. NOx and CO measurement demonstrated the emission capability and operability of the burner. Flame stability and lean/rich limits were identified for the primary and secondary flame. Modelling results were compared with experiments and flame characteristics (flame imaging by Chemiluminescence and OH-PLIF) were analyzed for the new fuel mixtures.

*I have calculated the operating condition (for new fuel mixtures) and led the experiment. Besides that, emission measurement and post processing, Chemiluminescence data collection and result post processing, CFD and chemical kinetics calculation and analysis were performed by me. A. A. Subash conducted the OH-PLIF measurement, post processing and still image acquisition. R. Collin and J. Klingmann supervised the experiment and paper writing.*

## Paper IX:

*Hydrogen Enriched Methane Flame in a Dry Low Emission Industrial Prototype Burner at Atmospheric Pressure Conditions*

By Arman Ahamed Subash, Robert Collin, Marcus Aldén, Atanu Kundu and Jens Klingmann

ASME Turbo Expo 2017: GT2017- 63924

The paper was based on the laser diagnostics of hydrogen enriched flames. OH-PLIF and Chemiluminescence images were utilized to investigate the flame shape and its variation with the change of operating conditions. Flame zone was identified from OH-PLIF probability distribution function results. The change in flame shape with the modification of fuel was analyzed in detail.

*As a co-author I have participated with the measurement campaign and assisted A. A. Subash for taking OH-LIF and Chemiluminescence images. I have decided the operating conditions and planned the test campaign. Apart from that I have supported with emission post processing and result interpretation. A. A. Subash was mainly responsible for post processing of the optical diagnostics images, capturing still images and writing the paper. M. Alden, R. Collin and J. Klingmann supervised the experiment and paper writing.*


## Paper X:

*Experimental Investigation of the Influence of Burner Geometry on Flame Characteristics at a Dry Low Emission Industrial Prototype Burner at Atmospheric Pressure Conditions*

By Arman Ahamed Subash, Robert Collin, Marcus Aldén, Atanu Kundu and Jens Klingmann

ASME Turbo Expo 2017: GT2017- 63950

This paper was based on the experimental campaign described in Paper VIII, mostly focused on laser diagnostics and image processing. The flame shape, local reacting zones and post flame regions were categorically explained by the OH-PLIF and Chemiluminescence imaging. As, OH concentration was a good marker for flame front and post flame zone, the results showed the effect of fuel mixture variation effect on flame length, flame stabilization point and its modification.

*As a co-author, my contribution is to plan and led the test campaign, selecting operating points and gas mixtures. I have helped A. A. Subash with emission result post processing and result interpretation. A. A. Subash is the lead author and he post processed all the optical diagnostics results and wrote the paper. M. Alden, R. Collin and J. Klingmann supervised the experiment and writing.*


## Paper XI:

*Flow Field Investigation of a Dry Low Emission Swirl Burner*

By Atanu Kundu, Jens Klingmann, Arman Ahamed Subash and Robert Collin

Manuscript ready for submission.

The paper was based on PIV measurement and its comparison with unsteady CFD simulation results. The PIV results were accumulated from isothermal and reacting flow field. With and without confinement effect were also analyzed. It was revealed

that recirculation zones (inner and outer) played significant role on flame stabilization of the prototype burner.

*I am the lead author for this paper. I have decided the operating condition and led the experiments. A. A. Subash helped me to set up the PIV system and participated with some measurements. I have performed PIV results post processing, CFD analysis and paper writing. R. Collin and J. Klingmann supervised the experiment and helped me to interpret the results.*

# CHAPTER 6: SUMMARY AND CONCLUSIONS

The doctoral thesis presented experimental and numerical investigation results on a downscaled prototype DLE burner. Multiple staging burner concept was the most attracting feature of this device for controlling emission and broadening operability. Along with temperature and emission measurements, sophisticated laser diagnostics techniques (2D OH-PLIF and 2D PIV) were applied. Numerical calculations (CFD and chemical kinetics) were performed for supporting the experimental findings and enhancing understanding of the combustion process. Based on the atmospheric investigation following conclusions could be made.

- The RPL stage experiment suggested that a rich RPL with lower residence time was advantageous for high concentration radical production (OH, O, CO and H) without NOx penalty. The High speed OH-PLIF image analysis showed strong axial fluctuation of the RPL flame.

- The full burner experiment explained the primary and secondary flame stabilization process. Two distinct flame anchoring regions were identified for the secondary flame (along the ISL and near the liner wall).

- Optical investigation (Chemiluminescence and OH-PLIF) indicated the flame front, post flame and maximum heat release region. A long secondary flame was observed inside the quartz liner. The flame length was reduced at higher flame temperature.

- Between 1680 K and 1780 K flame temperature, optimum operation of the burner was noticed with lower emission (NOx ~ 6 ppm). By reducing the RPL (RPL equivalence ratio ~ 0.6) combustion stoichiometry, less than 2 ppm NOx emission was noticed for the optimum operability range.

- A rich Pilot flame showed high NOx emission. A rich Pilot operation was helpful for CO oxidation in the lean operating conditions but showed minute effect at higher flame temperatures.

- The RPL and Pilot stage showed strong influence on secondary flame stabilization. Rich RPL and Pilot flames showed better flame stability.

- Pilot and RPL stage interaction displayed significant impact on NOx emission. NOx emission was also highly dependent on the RPL and Pilot stage stoichiometry.

- In the proximity of LBO, low frequency flame instability was observed. Recorded CO and UHC emission data showed high degree of fluctuation at lean operating conditions.

- A dominant frequency peak (411 Hz) was noticed at higher flame temperature. This could be related to the hot tone of the combustor.

- Flame stabilization (CRZ and ISL) locations were captured by the RANS CFD simulation. The emission results were compared with the model (CFD and CHEMKIN). A qualitative agreement was observed between the model and experiment.

- Geometrical change of the combustor inherently affected the aerodynamics of the flame zone. An ORZ region was created by eliminating the Quarl section from the combustor. A semi-stable intermittent flame in ORZ greatly affected the burner operability. Based on experiments Quarl section was highly recommended for better flame stability.

- The Dump configuration showed better CO oxidation performance. The RPL stage NOx contribution was estimated as 54 % of the total burner NOx.

- Up to 50 % hydrogen (by volume) blended fuel combustion tests were performed. The flame stabilization process and the anchoring location was unaltered with this fuel change. The flame length was reduced for high hydrogen flame since the turbulent flame speed was increased with the addition of hydrogen.

- NOx emission didn't show significant variation in the lean operating regime but a steeper growth was observed for high hydrogen fuels at higher flame temperature.

- LBO limits (primary and secondary flame) were extended for high hydrogen fuel blends. No significant effect of fuel change was noticed on the RPL and Pilot stage performance.

- OH-PLIF results indicated that OH concentration inside Quarl was increased linearly with hydrogen blending percentage. The LES simulated OH concentration was compared with the OH-PLIF image. The main flame topologies were captured by the simulation.

- Reacting and non-reacting flow field was investigated by 2D PIV and compared with the CFD simulation. The main flow topologies (CRZ, ORZ, ISL, OSL and the annular high speed jet) were captured by the

measurements. Axial velocity distribution and CRZ modification was observed for reacting case.

- The comparison of simulation and PIV measurement showed good agreement and trends. LES simulation showed better performance than RANS by capturing velocity distribution and eddies (different scales).

Overall, the experiments proved that the burner was capable of reducing emission (NOx < 9 ppm) with wide operability. The lean operation capability and high hydrogen fuel combustion supported advanced combustor design philosophy.

However, following areas need to be explored in future for getting better understanding of the combustion process.

- High pressure test is critical with detailed emission and dynamic pressure measurement capability.

- Simultaneous high speed LIF and PIV can be very useful for understanding the flame wrinkling and flame-turbulence interaction. High speed PIV can also address the seeding particle accumulation problem. As a significant part of the flame is stabilized closed to the liner wall, flame wall interaction study will be beneficial.

- The burner fuel flexibility experiments should be pushed further (with higher hydrogen %). A better stable liner (combustor) configuration (double walled air cooled) is essential for higher flame temperature experiments.

- Accurate CFD (LES) simulation considering realistic boundary condition and heat transfer is required to validate experimental results. Grid sensitivity study, combustion and turbulence model optimization for LES simulation should be performed.

# REFERENCES

[1] Agency, I. E., 2016, "World Energy Outlook 2016," International Energy Agency.

[2] GE, "Dry Low NOx 2.6+ Combustion Solution," https://powergen.gepower.com/services/upgrade-and-life-extension/heavy-duty-gas-turbine-upgrades-f-class/dry-low-nox-plus-2-6-combustion-solution.html.

[3] Siemens, "ULTRA LOW NOX COMBUSTION TECHNOLOGY," http://www.energy.siemens.com/mx/pool/hq/energy-topics/pdfs/en/gas-turbines-power-plants/PowerGen2008_UltraLowNoxCombustionTech.pdf.

[4] Candel, S., 2002, "Combustion dynamics and control: Progress and challenges," Proceedings of the Combustion Institute, 29(1), pp. 1-28.

[5] Huang, Y., and Yang, V., 2009, "Dynamics and stability of lean-premixed swirl-stabilized combustion," Progress in Energy and Combustion Science, 35(4), pp. 293-364.

[6] Boxx, I., Stöhr, M., Carter, C., and Meier, W., 2010, "Temporally resolved planar measurements of transient phenomena in a partially pre-mixed swirl flame in a gas turbine model combustor," Combustion and Flame, 157(8), pp. 1510-1525.

[7] Sadanandan, R., Stöhr, M., and Meier, W., 2008, "Simultaneous OH-PLIF and PIV measurements in a gas turbine model combustor," Applied Physics B: Lasers and Optics, 90(3-4), pp. 609-618.

[8] Steinberg, A. M., Boxx, I., Stöhr, M., Carter, C. D., and Meier, W., 2010, "Flow-flame interactions causing acoustically coupled heat release fluctuations in a thermo-acoustically unstable gas turbine model combustor," Combustion and Flame, 157(12), pp. 2250-2266.

[9] Weigand, P., Meier, W., Duan, X. R., Stricker, W., and Aigner, M., 2006, "Investigations of swirl flames in a gas turbine model combustor: I. Flow field, structures, temperature, and species distributions," Combustion and Flame, 144(1-2), pp. 205-224.

[10] Pitsch, H., 2006, "Large-eddy simulation of turbulent combustion," Annual Review of Fluid Mechanics, pp. 453-482.

[11] Selle, L., Lartigue, G., Poinsot, T., Koch, R., Schildmacher, K. U., Krebs, W., Prade, B., Kaufmann, P., and Veynante, D., 2004, "Compressible large eddy simulation of turbulent combustion in complex geometry on unstructured meshes," Combustion and Flame, 137(4), pp. 489-505.

[12] Driscoll, J. F., 2008, "Turbulent premixed combustion: Flamelet structure and its effect on turbulent burning velocities," Progress in Energy and Combustion Science, 34(1), pp. 91-134.

[13] Veynante, D., and Vervisch, L., 2002, "Turbulent combustion modeling," Progress in Energy and Combustion Science, 28(3), pp. 193-266.

[14] Stuttaford, P., Rizkalla, H., Oumejjoud, K., Demougeot, N., Bosnoian, J., Hernandez, F., Yaquinto, M., Mohammed, A. P., Terrell, D., and Weller, R., "FlameSheet™ Combustor Engine and Rig Validation for Operational and Fuel Flexibility With Low Emissions," Proc. ASME Turbo Expo 2016: Turbomachinery Technical Conference and Exposition, American Society of Mechanical Engineers, pp. V04AT04A040-V004AT004A040.

[15] Romoser, C. E., Harper, J., Wilson, M. B., Simons, D. W., Citeno, J. V., and Lal, M., "E-Class Late Fuel Staging Technology Delivers Flexibility Leap," Proc. ASME Turbo Expo 2016: Turbomachinery Technical Conference and Exposition, American Society of Mechanical Engineers, pp. V04BT04A050-V004BT004A050.

[16] Reddy, D. R., and Lee, C.-M., "An Overview of Low-Emission Combustion Research at NASA Glenn," Proc. ASME Turbo Expo 2016: Turbomachinery Technical Conference and Exposition, American Society of Mechanical Engineers, pp. V04AT04A003-V004AT004A003.

[17] Taamallah, S., Vogiatzaki, K., Alzahrani, F., Mokheimer, E., Habib, M., and Ghoniem, A., 2015, "Fuel flexibility, stability and emissions in premixed hydrogen-rich gas turbine combustion: Technology, fundamentals, and numerical simulations," Applied Energy, 154, pp. 1020-1047.

[18] Foley, C., Chterev, I., Seitzman, J., and Lieuwen, T., "Flame configurations in a lean premixed dump combustor with an annular swirling flow," Proc. 7th US National Combustion Meeting.

[19] Taamallah, S., Shanbhogue, S. J., and Ghoniem, A. F., 2016, "Turbulent flame stabilization modes in premixed swirl combustion: Physical mechanism and Karlovitz number-based criterion," Combustion and Flame, 166, pp. 19-33.

[20] Driscoll, J. F., and Temme, J., "Role of swirl in flame stabilization," Proc. 49thAIAA Aerospace Sciences Meeting including the New Horizons Forum and Aerospace Exposition, AIAA, pp. 1-11.

[21] York, W. D., Romig, B. W., Hughes, M. J., Simons, D. W., and Citeno, J. V., "Premixed Pilot Flames for Improved Emissions and Flexibility in a Heavy Duty Gas Turbine Combustion System," Proc. ASME Turbo Expo 2015: Turbine Technical Conference and Exposition, American Society of Mechanical Engineers, pp. V04BT04A067-V004BT004A067.

[22] Cohen, H., Rogers, G. F. C., Saravanamuttoo, H. I. H., and Saravanamutto, H., 1987, "Gas turbine theory."

[23] "Idealized Brayton cycle," https://en.wikipedia.org/wiki/Brayton_cycle#/media/File:Brayton_cycle.svg.

[24] Brooks, F. J., 2000, "GE gas turbine performance characteristics," GE Power Systems, Schenectady, NY.

[25] Jansohn, P., 2013, Modern gas turbine systems: High efficiency, low emission, fuel flexible power generation, Elsevier.

[26] Johnson, C., Pepperman, B., Koenig, M., Abou-Jaoude, K., Gulati, A., and Moradian, A., 2008, "Ultra low NOx combustion technology," PowerGen International. Siemens Power Generation Inc.

[27] Fric, T. F., 1993, "Effects of fuel-air unmixedness on NO (x) emissions," Journal of Propulsion and Power, 9(5), pp. 708-713.

[28] Eichler, C. T., 2011, Flame Flashback in Wall Boundary Layers of Premixed Combustion Systems, Verlag Dr. Hut.

[29] Law, C. K., 2010, Combustion physics, Cambridge university press.

[30] Peters, N., 2000, Turbulent combustion, Cambridge university press.

[31] Poinsot, T., and Veynante, D., 2005, Theoretical and numerical combustion, RT Edwards, Inc.

[32] Kolb, M., "Influence of the Injector Geometry on Mixing and Lift-Off of Premixed Jet Flames in Hot Cross Flow."

[33] Gupta, A. K., Lilley, D. G., and Syred, N., 1984, "Swirl flows," Tunbridge Wells, Kent, England, Abacus Press, 1984, 488 p., 1.

[34] Syred, N., 2006, "A review of oscillation mechanisms and the role of the precessing vortex core (PVC) in swirl combustion systems," Progress in Energy and Combustion Science, 32(2), pp. 93-161.

[35] Syred, N., and Beer, J., 1974, "Combustion in swirling flows: a review," Combustion and flame, 23(2), pp. 143-201.

[36] Lucca-Negro, O., and O'doherty, T., 2001, "Vortex breakdown: a review," Progress in energy and combustion science, 27(4), pp. 431-481.

[37] Kundu, A., Klingmann, J., Subash, A. A., and Collin, R., "Pilot-pilot interaction effects on a prototype DLE gas turbine burner combustion," Proc. Proceedings of the ASME Turbo Expo.

[38] Kundu, A., Klingmann, J., Subash, A. A., and Collin, R., "Flame stabilization and emission characteristics of a prototype gas turbine burner at atmospheric conditions," Proc. Proceedings of the ASME Turbo Expo.

[39] Kröner, M., Sattelmayer, T., Fritz, J., Kiesewetter, F., and Hirsch, C., 2007, "Flame propagation in swirling flows—effect of local extinction on the combustion induced vortex breakdown," Combustion Science and Technology, 179(7), pp. 1385-1416.

[40] Lieuwen, T. C., 2012, Unsteady combustor physics, Cambridge University Press.

[41] Benim, A. C., and Syed, K. J., 2014, Flashback Mechanisms in Lean Premixed Gas Turbine Combustion, Academic Press.

[42] Carrera, A. M., Andersson, M., and Näsvall, H., "Experimental investigation of the 4th generation DLE burner concept: Emissions and fuel flexibility performance at atmospheric conditions," Proc. ASME 2011 Turbo Expo: Turbine

Technical Conference and Exposition, American Society of Mechanical Engineers, pp. 1141-1148.

[43] Stöhr, M., Boxx, I., Carter, C., and Meier, W., 2011, "Dynamics of lean blowout of a swirl-stabilized flame in a gas turbine model combustor," Proceedings of the Combustion Institute, 33(2), pp. 2953-2960.

[44] Lieuwen, T. C., and Yang, V., 2005, "Combustion instabilities in gas turbine engines(operational experience, fundamental mechanisms and modeling)," Progress in astronautics and aeronautics.

[45] GE, https://powergen.gepower.com/content/dam/gepower-pgdp/global/en_US/documents/product/2016-gas-power-systems-products-catalog.pdf.

[46] Richards, G., McMillian, M., Gemmen, R., Rogers, W. A., and Cully, S., 2001, "Issues for low-emission, fuel-flexible power systems," Progress in Energy and Combustion Science, 27(2), pp. 141-169.

[47] Pavri, R., and Moore, G. D., 2001, "Gas turbine emissions and control," General Electric Report No. GER-4211.

[48] Lieuwen, T. C., and Yang, V., 2013, Gas turbine emissions, Cambridge University Press.

[49] AB, S. I. T., 2012, "The 37 MW Siemens SGT-750 approaches commercial application," http://pennwell.sds06.websds.net//2012/cologne/pgnp/papers/T3S3O4-paper.pdf.

[50] Städje, J., "Highly efficient and more than red hot - gas turbine is breathtaking engineering," http://techworld.idg.se/2.2524/1.663941/gasturbinen-hisnande-ingenjorskonst/sida/2/grundprinciper.

[51] Generation, S. P., "Gas Turbine SGT-750," http://www.energy.siemens.com/us/en/fossil-power-generation/gas-turbines/sgt-750.htm#content=Technical%20data.

[52] Milosavljevic, V., 2009, "Pilot combustor in a burner," Google Patents.

[53] Perel, D., 2013, "Innovation in Power Plants."

[54] ARP, S., 1996, "Procedure for the calculation of gaseous emissions from aircraft turbine engines."

[55] Ballester, J., and García-Armingol, T., 2010, "Diagnostic techniques for the monitoring and control of practical flames," Progress in Energy and Combustion Science, 36(4), pp. 375-411.

[56] Hardalupas, Y., and Orain, M., 2004, "Local measurements of the time-dependent heat release rate and equivalence ratio using chemiluminescent emission from a flame," Combustion and Flame, 139(3), pp. 188-207.

[57] Lee, J., and Santavicca, D., 2003, "Experimental diagnostics for the study of combustion instabilities in lean premixed combustors," Journal of propulsion and power, 19(5), pp. 735-750.

[58] Lauer, M. R. W., 2011, "Determination of the heat release distribution in turbulent flames by chemiluminescence imaging," Technische Universität München.

[59] Cheng, T.-S., Wu, C.-Y., Li, Y.-H., and Chao, Y.-C., 2006, "Chemiluminescence measurements of local equivalence ratio in a partially premixed flame," Combustion science and technology, 178(10-11), pp. 1821-1841.

[60] York, W. D., Ziminsky, W. S., and Yilmaz, E., 2013, "Development and testing of a low NOx hydrogen combustion system for heavy-duty gas turbines," Journal of Engineering for Gas Turbines and Power, 135(2), p. 022001.

[61] Linne, P. M. A., 2016, "https://www.princeton.edu/cefrc/combustion-summer-school/lecture-notes/Advanced-Laser-Diagnostics-in-Combustion-Research_Linne.pdf," https://www.princeton.edu/cefrc/combustion-summer-school/lecture-notes/Advanced-Laser-Diagnostics-in-Combustion-Research_Linne.pdf.

[62] Sadanandan, R., Stöhr, M., and Meier, W., 2008, "Simultaneous OH-PLIF and PIV measurements in a gas turbine model combustor," Applied Physics B, 90(3-4), pp. 609-618.

[63] Westerweel, J., Elsinga, G. E., and Adrian, R. J., 2013, "Particle image velocimetry for complex and turbulent flows," Annual Review of Fluid Mechanics, 45, pp. 409-436.

[64] Elsinga, G. E., Scarano, F., Wieneke, B., and van Oudheusden, B. W., 2006, "Tomographic particle image velocimetry," Experiments in fluids, 41(6), pp. 933-947.

[65] Schiwietz, T., and Westermann, R., "GPU-PIV," Proc. VMV, pp. 151-158.

[66] Samimy, M., and Lele, S., 1991, "Motion of particles with inertia in a compressible free shear layer," Physics of Fluids A: Fluid Dynamics (1989-1993), 3(8), pp. 1915-1923.

[67] Melling, A., 1997, "Tracer particles and seeding for particle image velocimetry," Measurement Science and Technology, 8(12), p. 1406.

[68] Raffel, M., Willert, C. E., Wereley, S., and Kompenhans, J., 2013, Particle image velocimetry: a practical guide, Springer.

[69] Sigfrid, I. R., Whiddon, R., Abou-Taouk, A., Collin, R., and Klingmann, J., "Experimental Investigations of an Industrial Lean Premixed Gas Turbine Combustor With High Swirling Flow," Proc. ASME 2012 Gas Turbine India Conference, American Society of Mechanical Engineers, pp. 559-569.

[70] ANSYS, A., 2009, "Academic research," Release.

[71] Fluent, A., 2016, "Influence of polyhedral mesh on gradient calculation," ANSYS.

[72] Fluent, A., "What is advantages of polyhedral mesh and method to get polyhedral mesh from hexa/tetra mesh."

[73] Fluent, A., 2009, "12.0 User's guide," 6.

[74] Fluent, A., 2009, "12.0 Theory Guide," Ansys Inc, 5.

[75] Wilcox, D. C., 1998, Turbulence modeling for CFD, DCW industries La Canada, CA.

[76] Menter, F. R., 2015, "Best Practice: Scale-Resolving Simulations in ANSYS CFD," ANSYS Germany GmbH.

[77] Design, R., 2010, "Chemkin-Pro 15101," Reaction Design, San Diego, CA.

[78] Turns, S. R., 1996, An introduction to combustion, McGraw-hill New York.

[79] Lefebvre, A. H., 1998, Gas turbine combustion, CRC press.

[80] Kundu, A., Klingmann, J., Subash, A. A., and Collin, R., "Pilot-Pilot Interaction Effects on a Prototype DLE Gas Turbine Burner Combustion," Proc. ASME Turbo Expo 2016: Turbomachinery Technical Conference and Exposition, American Society of Mechanical Engineers, pp. V04BT04A012-V004BT004A012.